ACADEMIA MATERIALS SCIENCE

Research Article
Published: 2024-07-17
https://doi.org/10.20935/AcadMatSci7277

Elucidation of novel, alternative, fiber-reinforced iron-based pozzolanic composites as SCMs

Hafiz Muhammad Nadir[1,*], Ash Ahmed[1], Ikram Moshi[1]

Academic Editor: Raul D.S.G. Campilho

Abstract

The researchers pioneered incorporating waste materials exhibiting pozzolanic properties and waste fibers from diverse industrial/agricultural fields into the construction industry to formulate enhanced, greener supplementary cementitious composites (SCMs). This research focused objectively on the formulation/evaluation of low-CO_2-embodied greener construction materials known as "novel, alternative, fiber-reinforced iron-based binary/ternary pozzolanic composites (abbreviated as NAFRIC)". The composites incorporated iron powder (Fe), metakaolin (MK), pulverized fly ash (PFA), ground granulated blastfurnace slag (GGBS), palm ash, silica fume, and limestone, which are anticipated to absorb CO_2 while producing siderite (ferrous carbonate $FeCO_3$). All the NAFRIC mixes formulated in this study demonstrated up to 4–13% improvement in compressive strength and 70–130% in flexural strength with an enhanced rupture modulus/post-crack ductility. The ternary pozzolanic iron-based fiber-reinforced concrete (FRC) composites containing 8% MK + 10% PFA + 10% GGBS and steel/polypropylene/polyethylene terephthalate (PET) fibers performed the best with attaining up to 70 MPa compressive and up to 8.9 MPa flexural strengths. The sulfate testing evaluated the durability of NAFRIC SCMs formulated in a 1:2:3 ratio better than cement concrete control mix with a 1:1:3 ratio. NAFRIC specimens demonstrated minimal surface deterioration/elongation and negligible/no strength reduction after 270 days of concentrated sulfate attack. The microstructural analysis using X-ray diffraction/fluorescence, scanning electron microscopy/energy-dispersive analysis with X-ray spectroscopy supported the strength and durability parameters by showing minimal/no ettringite formation and increased calcium silicate hydrates gel formation due to the use of $FeCO_3$ and pozzolans. The study demonstrated the sustainable use of these better-performing NAFRIC SCMs with 10–12% reduced embodied CO_2 as eco-friendly high-strength SCMs with enhanced engineering/environmental benefits.

Keywords: *iron, pozzolans, FRC, NAFRIC SCMs, durability, embodied CO_2.*

Citation: Nadir HM, Ahmed A, Moshi I. Elucidation of novel, alternative, fiber-reinforced iron-based pozzolanic composites as SCMs. *Academia Materials Science* 2024;1. https://doi.org/10.20935/AcadMatSci7277

1. Introduction

1.1. Background

The CO_2 emission from ordinary portland cement (OPC) manufacturing, raw materials quarrying, and transportation is estimated to be around 10% of global emissions (0.8–0.9 tons of CO_2 per ton of cement manufacturing), making the construction industry the second most significant contributor to global warming and depleting natural resources. The earth is facing another challenge of increased production/disposal of waste materials from industries, agricultural, and domestic fields. Waste production has intensified manifold in the last few decades due to technological advancements, increased world population, and inventions of new materials and is estimated to reach more than 2.2 billion metric tons annually by 2025 [1–9]. The global greenhouse gas (GHG) emissions from cement concrete manufacturing can be divided into five phases. In the first phase, the mining, extraction, and calcination of cement raw materials, fine and coarse aggregates, and manufacturing of admixtures (including air entertainers, plasticizers, accelerators, retarders, and curing compounds) are the significant CO_2 emitting processes (up to 75–85%). The second phase accounts for up to 6% of emissions, including national/international transportation of cement/other ingredients. The third phase is mixing concrete ingredients in the in situ/onsite or at the concrete plants away from the construction sites. The fourth phase is transporting fresh concrete from the plants to the construction sites using transit mixers. The fourth and fifth/final phases are responsible for up to 10–15% of CO_2 emissions and include the transportation, placement of concrete for construction using formwork, concrete pumps, vibrators, curing, hydration, ultimately demolition, and then recycling it to use as recycled aggregates as useful waste disposal [10]. Concrete main ingredients are binder (cement responsible for up to 80% of GHG emissions), fine/coarse aggregate (responsible for up to 5% GHG emissions), admixtures (responsible for up to 2% GHG emissions), and water (zero emissions) [1, 3, 7, 10–12]. The use of cement alternatives/partial replacement composites is the foremost applicable solution to reduce the carbon footprints of the construction

[1]Civil Engineering Group, School of Built Environment & Engineering, Leeds Beckett University, Leeds LS2 8AG, UK.
*email: hafiznadir786@gmail.com

industry by 30–50%, as stipulated in 28th conference of parties on climate (COP28) for 2030 and 2050 targets [13–18]. Consequently, the ongoing research converges on the formulation of greener, eco-friendly, economical, waste-absorbent, and low resource-consuming supplementary cementitious composites (SCMs) demonstrating sustainable/comparable engineering properties. Using fibers of diverse materials like steel fibers (STF), polypropylene fibers (PPF), polyethylene terephthalate (PET), coconut coir fibers (COF), and wheat straw fibers (WSF) is a beneficial option to improve crack prevention and tensile/flexural strength in concrete [1, 10, 19]. An iron-based pozzolanic material, "ferrock", presumably a low energy consuming, CO_2 negative balance creator, and lower global warming potential (GWP) material, was formulated incorporating the iron powder (Fe) and pozzolans. Iron powder (Fe) converts into rock-like ferrous carbonate ($FeCO_3$), and other ingredients like silica (SiO_2), pozzolans, and lime ($Ca(OH)_2$) convert into calcium silicate hydrates (C-S-H) gel after completion of the pozzolanic reaction [8]. The generic ferrock was formulated using 60% Fe, 20% pulverized fly ash (PFA), 8% metakaolin (MK), and 12% limestone ($CaCO_3$), exhibiting at par or even better engineering properties than OPC concrete [8, 19]. The researchers have suggested beneficial use of pozzolans as filler material for pore refinement and strength enhancer with increased production of C-S-H gel but restricting their use up to some specific/limiting dosages for different pozzolanic/cement replacement materials (ground granulated blastfurnace slag (GGBS) up to 70–80%, PFA up to 40%, MK up to 20%, silica fume (SF) up to 15%, and PA up to 10%). The higher silica contents in these materials tend to produce calcium silica hydrates after the transformation of SiO_2 into aqueous SiO_2 and further to alkaline calcium silica hydroxide gel, which possesses swelling properties and can initiate cracking in the SCMs [1, 7, 19, 20, 21–29].

1.2. Cement hydration process

The cement is an anhydrous material and contains no strength in dry form and requires water mixing to initiate a complex hydration process involving the conversion of its constituent chemical compounds into calcium-silicate-hydrate (C-S-H) gel responsible for the characteristic strength of concrete. (Equation 1 shows the conversion of trisilicates into C-S-H gel on hydration.) Trisilicates and disilicates are responsible for the initial strength [25], the pozzolanic reaction of silica and $Ca(OH)_2$ (Equation 2) [26], conversion of Fe into $FeCO_3$ (Equation 3) [19], and conversion of excess silica into swelling/cracking calcium-silica hydrate ($CaO{\cdot}Si(OH)_4$) (Equations 4–6) [26], and all of these are elaborated in the chemical equations below:

$$2\left(3CaO{\cdot}SiO_2\right)+6H_2O \rightarrow 3CaO{\cdot}2SiO_2{\cdot}3H_2O+3Ca(OH)_2+\text{Heat} \quad (1)$$

$$2SiO_2+3Ca(OH)_2 \rightarrow 3CaO{\cdot}2SiO_2{\cdot}3H_2O \quad (2)$$

$$Fe+CO_2+H_2O \rightarrow FeCO_3+H_2\uparrow \quad (3)$$

$$SiO_2+2Ca(OH)_2 \rightarrow Si(OH)_4{\cdot}2CaO \quad (4)$$

$$SiO_2+2H_2O \rightarrow Si(OH)_4 \quad (5)$$

$$Si(OH)_4+2Ca(OH)_2 \rightarrow Si(OH)_4{\cdot}2CaO+2H_2O \quad (6)$$

1.3. Iron-based binary/ternary pozzolanic SCMs

A previous study by the authors on formulating iron (Fe)-based binary/ternary pozzolanic plain SCMs with 10–50% OPC in a 1:2:3 ratio demonstrated better compressive/flexural strengths than high-strength M60 grade plain cement concrete (PCC) 1:1:3 (60 MPa) as shown in **Figure 1** [19]. All 10–50% SCMs with Fe-based pozzolanic combinations reached the target strength of C32/40 or M40 concrete at 28 and 91 days of curing, demonstrating an overall increase of up to 12% compressive strength and 5% flexural strength [19]. The increased dosage of Fe-based SCMs with OPC increased the ductility of prisms/beams. It resulted in increased flexural strength/post-crack ductility due to the characteristic ductility of iron particles [7, 19, 20]. Contemporary research supports the sustainable use of Fe-based pozzolanic SCMs as a full/partial greener alternative to OPC [19]. Vijayan et al. [21] evaluated that 4–12% Fe replacement with OPC exhibited better engineering properties, with 8% as the optimum dosage. Karthika and Leema [22] elucidated the impacts of using 5%, 10%, 15%, 20%, and 25% Fe replacement with OPC. They suggested 10% as the optimum dosage, demonstrating the durability in sulfate attack and the best mechanical properties among all the mixes/ratios of SCMs. Prashanth et al. [23] investigated the use of oxalic acid $C_2H_2O_4$ or $(COOH)_2$ as a catalyst to increase the formation of $FeCO_3$ with conventional Fe and found that up to 12 moles of this weak organic acid can enhance the chemical reaction; however, cost-benefit analysis of using oxalic acid at 2–12 moles/m^3 of concrete volume evaluated 2% as the most economical/feasible dosage of oxalic acid [19, 23, 24].

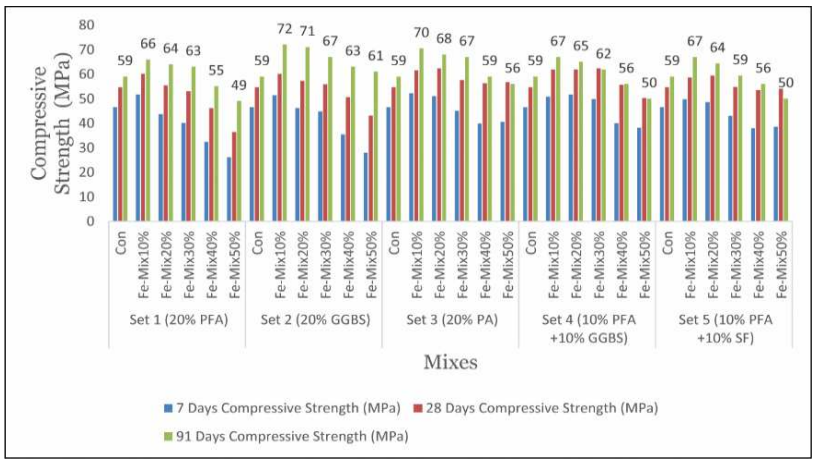

Figure 1 • Comparison of compressive strength—sets 1–5, 10–50% replacement of OPC with plain iron-based pozzolanic SCMs [19]. All the SCMs exhibited up to 50–70 MPa strength.

1.4. Iron-based fiber-reinforced pozzolanic composites (NAFRIC)

A noticeable work has been conducted exploring mechanical properties and chemo-mechanical synthesis of iron-based materials/composites; however, more work to evaluate engineering properties, microstructural analysis, incorporation of waste fibers, and analysis of embodied carbon footprints/cost has yet to be undertaken on formulating/evaluating these novel materials, indicating a research gap. An effort has been made to measure the research/practical gap by formulating/recycling sustainable waste material/fibers to protect the environment. Therefore, this study has been conducted to elucidate the impacts of mixing 10% and 17% of STF, 1% and 2% of PPF as established materials, and 1% and 2% of PET plastic fibers and WSF as better-performing "novel, alternative, fiber-reinforced iron-based binary/ternary pozzolanic composites (NAFRIC)". 10% of Fe-based pozzolanic mix and 90% of OPC-based SCMs containing the binary pozzolans (8% MK with 20% PFA or 20% GGBS or 20% palm ash (PA)) and the ternary pozzolans (8% MK + 10% PFA + 10% GGBS or 8% MK + 10% PFA + 10% SF) have been evaluated setting a target characteristic compressive strength of C32/40 or M40 concrete (≥40 MPa).

1.5. Durability against sulfate attack

Cement concrete with higher sulfate contents, higher w/c ratio of more than 0.45, increased permeability due to porous structure because of aeration/voids, excessive moisture, and contact with the marine environment and saltish soils are some of the significant causes of sulfate attack. Pozzolans, sulfate-resistant cement, and other preventive measures like surface protection/coating can reduce the chances of attack [4, 30–35]. Sulfate attack by Na_2SO_4 solution is characterized by causing elongation in the concrete specimens. In contrast, sulfate attack by $MgSO_4$ is considered an internal attack by producing long, needle-like ettringite crystals, which cause cracking and failure of the structure. The cations Mg^{++}/Na^{+} and Ca^{++} exchange, and the anions SO_4^{--} and OH^{-} exchange. The sulfate ion SO_4^{--} from magnesium/sodium sulfate transfers inward to form gypsum $CaSO_4$, whereas the OH^{-} ion from $Ca(OH)_2$ exchanges outward to form brucite $Mg(OH)_2$ or NaOH (Equations 7 and 8) [25, 26].

$$Ca(OH)_2 + MgSO_4 + 2H_2O = CaSO_4 \cdot 2H_2O + Mg(OH)_2 \quad (7)$$

$$Ca(OH)_2 + Na_2SO_4 + 2H_2O = CaSO_4 \cdot 2H_2O + 2NaOH \quad (8)$$

The gypsum and brucite produced during external $MgSO_4$ attacks initially make a membrane around concrete ingredients to save from sulfate attacks. However, later, the presence of gypsum ($CaSO_4 \cdot 2H_2O$) initiates the formation of ettringite ($3CaO \cdot Al_2O_3 \cdot CaSO_4 \cdot 32H_2O$) by reacting with monosulfate aluminum hydrate ($3CaO\ Al_2O_3 \cdot 3CaSO_4 \cdot 12H_2O$), which causes peeling of this membrane and propagatesinward, cracking inside the concrete mass (Equation 9—not balanced) [25, 26].

$$CaSO_4 \cdot 2H_2O + 3\left(3CaO \cdot Al_2O_3 \cdot 3CaSO_4 \cdot 12H_2O\right) + H_2O = 3CaO \cdot Al_2O_3 \cdot CaSO_4 \cdot 32H_2O \quad (9)$$

The diffusion/exchange of Mg^{++} cation with Ca^{++} of calcium silicate hydrates (C-S-H gel) forms magnesium silicate hydrates (M-S-H gel) [30]. M-S-H gel does not possess any strength or binding properties. It causes a reduction in the compressive strength of concrete by reducing intra-ingredient binding (Equation 10) [25, 26, 36].

$$3CaO \cdot 2SiO_2 \cdot 3H_2O + 3MgSO_4 + 2H_2O = 3MgO \cdot 2SiO_2 \cdot 3H_2O + 3CaSO_4 \cdot 2H_2O \quad (10)$$

The decrease in intra-ingredients binding and formation/propagation of cracks by long needle-like crystals of ettringite let the sulfate diffuse deep inside and slowly/gradually spread this sulfate attack in all dimensions of concrete mass, failing/collapsing the total concrete structure. The increased presence of Ca^{++} highly influences the typical internal sulfate attack $(OH)_2$ [37], tricalcium aluminates C_3A (celite) [38], and monosulfate aluminate hydrate ($3C_4ASH_{18}$) [36], which contains a single molar SO^{-}_3 [39], and converts readily to ettringite on the formation of gypsum during sulfate attack [25, 26, 36].

2. Materials

2.1. Cement, aggregate (coarse and fine), and plasticizer

CEM 1 52.5, white cement conforming to BS EN 197-1/2011 [40], has been used for this study. CEM1 achieves a target characteristic compressive strength of 52.5 MPa at 28 days of curing and contains 67.1% CaO, 25.2% SiO_2, and 7.7% other metals' oxides as evaluated through elemental X-ray diffraction (XRD) analysis (**Table 1**). Angular/crushed coarse aggregate passing through a 20-mm sieve and fine aggregate extracted from river sand passing a 4-mm sieve have been used for this study, conforming to BS EN 12620/2013 [41]. The aggregates impart intra-ingredient bonding with the binder to achieve the target characteristic compressive strength of novel SCMs [19]. The mixes have been prepared using a mix ratio of 1:2:3 with a water-cement ratio (w/c) of 0.35 (by the total weight of binder). A carboxylate polymer-based plasticizer has been used from 0.2% to 0.25% of the binder's total weight to maintain the consistency of self-compacting concrete.

2.2. Iron powder (Fe) and the cement replacement/pozzolanic materials

Iron powder is finely grained iron particles of 19–24 μm, produced as waste under the blast furnace floor during shot blasting of scrap steel. The typical iron powder contains 93% Fe (**Table 1**) with a specific density of 2.8 g/cm^3 and is considered a hazardous material with significant environmental impacts. Its consumption as iron oxide powder for coating metal surfaces is extensively used in different sectors. There has been a rise in the use of iron-based SCMs as greener materials in the construction industry for the last ten years [19, 42–44]. As per ASTM C 618/C125-19 [45], an excellent pozzolanic/cement replacement material should contain an accumulated sum of more than 60% of silica, alumina, and other metals' oxides to be used as partial/complete replacement of cement. Therefore, only the materials exhibiting/containing pozzolanic performance/ingredients conforming to ASTM C 618/C125-19 have been used in this study. As discussed earlier, the silica in the pozzolans reacts with the portlandite $Ca(OH)_2$ produced during the hydration of OPC to produce additional C-S-H gel, contributing to gaining further strength. Using pozzolans in OPC concrete improves the engineering properties by increasing pore refinement, ductility, compressive/flexural strength, and durability against sulfate

attack and by decreasing permeability, alkali-silica effects, and shrinkage [6, 19]. However, excessive pozzolans can produce swelling calcium silica hydrates, thus weakening the concrete and limiting their use to specified/feasible ratios [19, 25, 26]. GGBS is an established and broadly used direct cement replacement material demonstrating at-par performance with the OPC. It contains 44.7% CaO, 39.4% SiO_2 and 11.1% Al_2O_3 (**Table 1**) and is obtained as a waste slag from the steel blast furnace industry. GGBS is an off-white color powder exhibiting a specific gravity of 2.9, fineness of 350 m^2/g and vibrated bulk density of around 1,300 kg/cm^3 [1, 2, 19, 46–48]. 20% PFA and 8% MK are used to prepare conventional Fe [8, 19]. However, this study used modified Fe with 20% GGBS and 10% GGBS + 10% PFA instead of 20% PFA to develop novel fiber-reinforced Fe-based SCMs. PFA is obtained from coal power plants as a waste material with a particle size of 0.5–300 µm and contains 56.2% SiO_2, 23.7% Al_2O_3, and 8.88% Fe_2O_3 (**Table 1**) [26, 49–52]. MK is an amorphous crystalline material chemically composed of dehydroxylated aluminum silicate ($Al_2O_3{\cdot}2SiO_2{\cdot}2H_2O$), obtained by calcinating naturally occurring Kaolinite clay mineral under 450–650 Celsius. It contains 52.1% SiO_2 and 45.1% Al_2O_3 (**Table 1**), making it a suitable pozzolan per ASTM standards C 618/C125-19 [1, 53]. SF is the most silica-containing amorphous crystalline pozzolan (99.1% **Table 1**), obtained as waste material from the arc furnace while manufacturing silicon/ferrosilicon products [1, 54, 55]. This study has used 10% SF with 10% PFA as modified ternary pozzolanic Fe-based SCM instead of 20% PFA of conventional Fe. PA is the waste product of the palm oil industry and is obtained by burning palm, leaves, and branches at 700°C. The ash contains 62.5% silica and 19% CaO. PA contains 2% K_2O, which imparts cracking to concrete, and the researchers suggest PA's careful use to specified limits [1, 56–58]. This study used 20% PA with 8% MK as binary pozzolanic Fe-based SCM instead of 20% PFA of conventional Fe. In total, 2% oxalic acid (by the weight of binder) has been used as a catalyst to increase the Fe^{++} reaction with CO_3^{--} to produce $FeCO_3$ in Fe-based SCMs [24]. Lime is a white powder of particles around 4 µm with a vibrated bulk density of 1,100 kg/m^3 and has been used as a cementing material since pre-history times [7, 25, 59]. 12% limestone has been added to impart Ca^{++} ions for the formation of slacked lime $Ca(OH)_2$ to form additional C-S-H gel during the pozzolanic reaction and to supply CO_3^{--} ions to react with Fe^{++} to form rock-like $FeCO_3$ during carbonation of Fe. These chemical reactions contribute to the additional strength of frock-based SCMs [19]. The cement replacement materials and fibers are illustrated in **Figure 2**.

Table 1 • Elemental/ingredient composition analysis by XRD/refractometry of different materials

Ingredients	CEM1 (%)	GGBS (%)	SF (%)	MK (%)	Fe (%)	PFA (%)	PA (%)
Fe_2O_3	0.32	0.31	0.43	0.45	93	8.88	3.12
SiO_2	25.2	39.4	99.1	52.1		56.2	62.5
TiO_2	0.18	0.47	<0.1	0.88		0.83	0.12
CaO	67.1	44.7	<0.1	0.31		3.46	19
K_2O	0.30	0.43	<0.1	0.17		0.66	2.0
Al_2O_3	3.18	11.1	<0.1	45.1		23.7	4.5
MgO	1.33	1.46	<0.1	0.20		3.28	1.18
Na_2O	<0.1	0.11	<0.1	0.25		1.93	<0.1
P_2O_5	<0.11	<0.1	<0.1	<0.1		<0.31	<0.1
Cl	<0.23	<0.1	<0.1	<0.1		<0.1	<0.1
SO_3	<1.57	<1.49	<0.1	<0.1		0.25	0.53
O_2					6		

2.3. The fibers

The use of fibers to improve the strength of construction materials, for example, animal wool/hair and agricultural straw fibers from plants and coconut coir, has been used by ancient civilizations like the Sumerians, Babylonians, and Egyptians [1, 60]. The researchers endeavor to introduce micro/macrofibers of different waste materials to give eco-friendly/economical solutions [1]. However, using fibers in concrete is evaluated as feasible within a specific optimum ratio based on the fibers' nature/and aspect ratio. Incorporating fibers beyond optimum dosage may decrease concrete's compressive strength [1, 9, 60–71]. Steel is an established material used as reinforcement in concrete, such as bars, mesh, and fibers. Straight, crippled, or hooked STF are ductile, strong, heat/crack resistant but corrosion-prone fibers obtained as a steel industry waste by shredding/cutting steel sheets, meshes, and wires from electric cables/rubber tires. The fibers with 0.2 mm diameter and 10–60 mm length exhibit a tensile strength of 400–2,200 MPa, Young's modulus of 200 GPa, and a 7,800 kg/m^3 density. Their established dosage of 10% (40 kg/m^3) and 17% (60 kg/m^3) has been evaluated as the best-performing ratio by the researchers [1, 72–74]. Polypropylene is another established material for fiber reinforcement in concrete. It is derived from 85% propylene monomer as stereognosis thermoplastic micro/macrofibers having 0.2–0.5 mm diameter and 10–50 mm length exhibit a tensile strength of 300–800 MPa, Young's modulus of 3.5–10 GPa, elongation of 30–100%, and a density of 0.9 g/cm^3. The researchers elucidated 1% (4 kg/m^3) to 2% (8 kg/m^3) as the optimum dosages, suggesting it as the best-performing non-metal material due to its no water absorption, super elongation, and corrosion-free usage [1, 75–77]. Today, PET plastic bottles/packings are used in every industry/household. The challenge of disposing of around a million

tons/day of worldwide PET waste, including using around 20,000 plastic bottles per second, is an enormous environmental hazard necessitating an effective strategy to reuse/recycle. The shredded PET fibers having 1–5 mm diameter and 50–200 mm length exhibit a tensile strength of around 270–300 MPa, Young's modulus of 2–3 GPa, elongation of 30–40%, and a density of 1.4 g/cm^3, with no water absorption, super elongation, and corrosion free usage. Since their optimum dosage is yet to be established, a proposed dosage aligning to the use of PPF with 1% (4 kg/m^3) and 2% (8 kg/m^3) ratios has been incorporated in this study to demonstrate at-par performance with PPF [1, 9, 61, 78–81].

Wheat straw is made from shredded stems of harvested wheat plants of 2–3 mm diameter containing up to 40% cellulose, 20% moisture, and 30% lignin/pectin with traces of ash, demonstrating a tensile strength of around 20–30 MPa, a rigidity modulus of 260–500 MPa, an elongation of 5–10%, and a shear strength of 4–7 MPa. These properties propose WSF to be a feasible fiber for concrete reinforcement; however, its water absorption capacity, lesser elongation, more significant aspect ratio, and lignin/pith limit its use to minimum percentages of 1–2% as increased quantities seriously hamper the compressive strength and post crack ductility [1, 82–84].

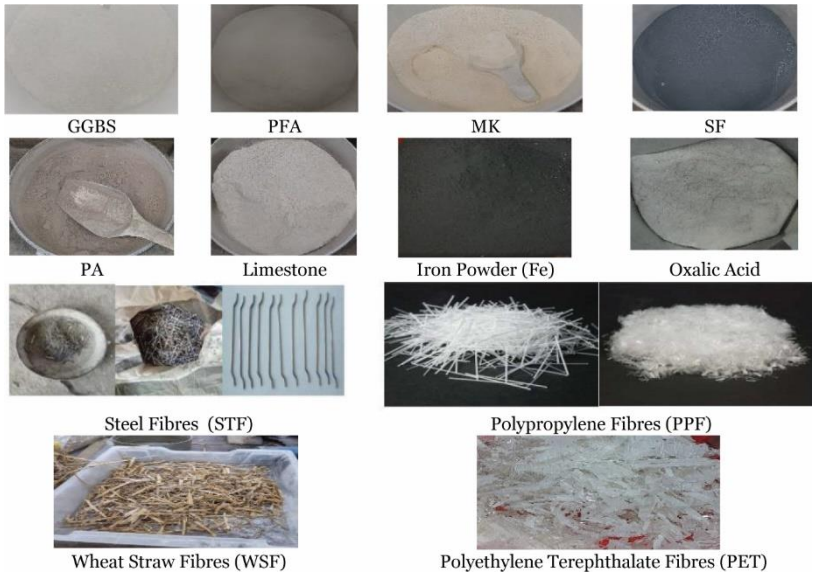

Figure 2 • Cement replacement/pozzolanic materials and fibers used in this study.

3. Methods

3.1. Formulation of NAFRIC mixes

This study has been conducted to elucidate the impacts of mixing established fibers like 10% and 17% STF, 1% and 2% PPF, and 1% and 2% innovative fibers like PET and WSF with the best performing 10% conventional/modified Fe-based SCMs containing the binary pozzolans/ternary pozzolans. Sets 1–3 contain Fe with binary pozzolans, that is, 8% MK with 20% PFA (set 1), 8% MK with 20% GGBS (set 2), and 8% MK with 20% PA (set 3), respectively. Sets 4 and 5 contain Fe with ternary pozzolans, that is, 8% MK with 10% PFA + 10% GGBS (set 4) and 8% MK with 10% PFA + 10% SF (set 5), respectively, as shown in **Table 2**. The control mixes containing PCC without Fe/fibers (with a ratio of 1:1:3) and 10% conventional/modified Fe-based cement composites without fibers (with a ratio of 1:2:3) have been prepared for comparison. The mixes have been formulated using CEM1 52.5 with coarse/fine aggregates and 10% Fe/pozzolans, 90% OPC, and 1–2% fibers mixing as fiber-reinforced concrete (FRC) with a 1:2:3 mix ratio in conformance with BS EN 12620/2013 [41].

Table 2 • Composition of conventional/modified iron (Fe)-based binary/ternary pozzolanic NAFRIC SCMs with 10% Fe replacement—sets 1–5

Material	Set 1—Fe-composites with 20% PFA (%)	Set 2—Fe-composites with 20% GGBS (%)	Set 3—Fe-composites with 20% PA (%)	Set 4—Fe-composites with 10% PFA + 10% GGBS (%)	Set 5—Fe-composites with 10% PFA + 10% SF (%)
Iron powder	60	60	60	60	60
PFA	20	–	–	10	10
GGBS	–	20	–	10	–
PA	–	–	20	–	–
SF	–	–	–	–-	10
MK	8	8	8	8	8
Limestone	10	10	10	10	10
Oxalic acid	2	2	2	2	2

3.2. Physical/mechanical properties testing

The standard cone and rod apparatus was used to measure the slump to ascertain workability (**Figure 3a**) with the target S1 slump as per BS EN 8500 [10, 19, 85]. The 100-mm cubes have been prepared/tested for compressive strength at 28, 91, and 270 days in conformance with BS EN 12390-2:2019 on the compressive testing machine shown in **Figure 3b** [86]. The 500 mm × 100 mm × 100 mm prisms/beams have been prepared/tested for flexural strengths at 91 days as per BS EN 12350-1 and were tested on a flexural testing machine (Premier Farnell Limited, Leeds, UK) with manual hydraulic three-point loading, as shown in **Figure 3c** [87]. The target characteristic compressive strength of C32/40 or M40 concrete [35, 87–89] has been set to be achieved by the mixes of this study. The density has been calculated as per BS EN 12390-7:2019. The flexural strength has been drawn versus the displacement/width of the prism's crack after applying bending load on a point flexural loading machine to ascertain the post-crack ductility of specimens. The specimens exhibiting more strength and displacement while remaining intact even after rupture are classified as more ductile, demonstrating prolonged post-crack utility. Carbonation of NAFRIC SCMs has been ascertained by applying phenolphthalein spray at the center depth of the cubes to assess the presence of CO_2 after 28, 91, and 270 days of curing. A dark pink color shows the presence of CO_2, which can result in the corrosion of the reinforcement. The light pink or no color shows slight or no availability of CO_2, indicating the absorption of CO_2 by NAFRIC to form $FeCO_3$.

Figure 3 • (a) Slump testing, (b) compressive testing machine (Impact Test Equipment Ltd, Stevenston, UK) for testing of 100-mm cubes, and (c) three-point loading flexural testing equipment for 500 mm × 100 mm × 100 mm prisms/beams.

3.3. Sulfate resistance testing

The durability of materials can be ascertained by analyzing the performance of composites against external sulfate attack by immersing 100-mm cubes in a 2.5% Na_2SO_4 + 2.5% $MgSO_4$ solution for ≥270 days under laboratory conditions, imitating 20 years of field exposure in natural conditions. American Society for Testing and Materials C1012/C1012M–15:2018 specifies the testing procedure for assessment of durability/resistance of concrete against sulfate attack. BS EN 206:2013+A2:2021 specifies the required performance of composites and concrete [31, 34, 35]. The cubes or tiny prisms are kept in a 5% sulfate concentrated solution (50 g/L of Na_2SO_4 or $MgSO_4$ or H_2SO_4 or combinations) after attaining 20 MPa strength for a prolonged period to replicate the field attack of 10–20 years in controlled conditions of the laboratory. The cubes were immersed in a water tank and a sulfate solution in a combined 2.5% Na_2SO_4 + 2.5 $MgSO_4$ solution for 270 days. The solution was refreshed every three months, along with cubes exposed to dry/wetting field-like conditions. The cubes were tested for compressive strength after 270 days of sulfate exposure to compare strength variation with those cured in water for 270 days.

3.4. Micro-structural testing

The physio-mechanical properties of NAFRIC SCMs like consistency, density, physical appearance, compressive strength, flexural strength, carbon dioxide absorption, durability against sulfate attack, surface deterioration/elongation due to sulfate attack, microstructural analysis using XRD/scanning electron microscopy (SEM, Hitachi High-Technologies Corporation Tokyo, Japan), and assessment of their embodied CO_2 with cost-benefit analysis have been elucidated to evaluate the suitability of these novel composites (details of testing have been covered in succeeding sections along with discussions). Sustainable composites developed as greener SCMs by this study incorporating waste material with cement/lime/iron powder/pozzolans/fibers are expected to reduce global waste production and minimize CO_2 emissions by the construction industry by at least 10–12%. This study conducted X-ray fluorescence (XRF Philips, Amsterdam, The Netherlands) analysis to ascertain the elemental composition of various pozzolanic materials and OPC in oxides. The crushed specimens of the selected NAFRIC (F/PFA/SF PET1% and F/PA PET1%) composites, after 270 days of sulfate exposure, were ground to particles of size less than 150 µm using a ball mill, heated up to 975°C, tested for loss of ignition, and then analyzed for several elements using a Philips Minipal 4 EDXRF (Amsterdam, The Netherlands) machine to assess the elemental configuration through XRF as oxides of metals. A section from each specimen's slices was mounted, coated, and examined by SEM and energy dispersive analysis with X-ray spectroscopy (EDAX) under various magnifications using an SEM machine and getting microfabric/crystallographic results in the attached visual display monitor as images and energy-dispersive X-ray spectroscopy (EDS) spectrum. The images and EDS spectrum can be used to analyze the crystalline/amorphous morphology of the specimen with up to 25,000× magnification, showing the presence of different compounds, which can be identified by matching these to an AMCSD-like database by SEM experts, augmented by EDS spectrum quantifying the exact percentage presence of various compounds in the given specimen.

4. Results and discussion

4.1. Density

The density of the cubes exhibited less impacted/varying statistics with the use of different fibers/NAFRIC compositions. Generally, all the cubes demonstrated a normal concrete density range between 2,200 and 2,500 kg/m³ (**Figure 4**), based on the nature of the materials, types of fibers, and degree of compaction.

An increase of up to 4% density was observed with increased age of curing up to 91 days with increased water absorption. A decrease of up to 2.5% density was observed in composites containing 2% WSF, probably because of the lesser weight of WSF versus other fibers. The maximum density was demonstrated by the composites containing STF and GGBS, obviously due to the heavy dosage and weight of STF and the higher unit weight of GGBS. BS EN 12390-7:2019 [90] provides guidelines to ascertain the density of concrete and classify it into three categories: light- (800–2,000 kg/m³), regular- (2,000–2,600 kg/m³), and heavy-density concretes (>2,600 kg/m³) [90]. The density of all the materials under study was calculated using dry mass M_d of 100-mm cubes in the air on digital balance, and then the same cube was weighed in water, taking M_w (the mass of cubes in water). The density has been calculated using Equation 11 and was found under the regular density range of 2,200–2,600 kg/m³:

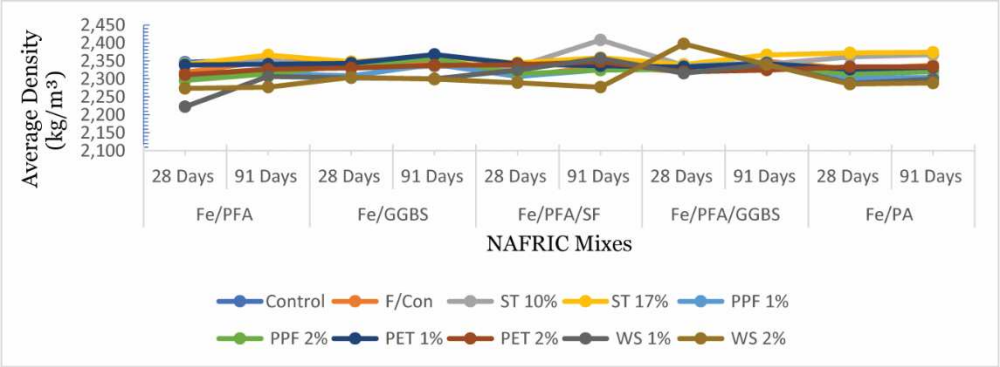

Figure 4 • Comparison of 28 and 91 days average density—NAFRIC mixes. All the mixes exhibited a normal density range of 2,200–2,600 kg/m³.

$$\text{Density}\,(D) = \left[M_d / \left(M_d - M_w \right) \right] \times 1{,}000 \qquad (11)$$

where M_d is the dry mass of cubes in air and M_w is the mass of cubes in water.

4.2. Workability

The consistency of all the mixes/specimens was ascertained using slump testing using standard cone and rod apparatus (**Figure 3a**) with target S1 slump as per BS EN 8500 and BS EN 12390-2:2019 [41, 90]. A true slump of 10–40 mm was targeted during the study while keeping the w/c ratio to 0.35 for cement concrete control mix and iron-based pozzolanic SCMs (NAFRIC) using 0.2–0.25% plasticizer. Generally, all the Fe-based FRC composites exhibited a decreased workability on the mixing of fibers/NAFRIC; therefore, 10–25 ml plasticizer (by the weight of total binder) was used with the mixes to get a self-compacting consistency/workability.

4.3. Compressive strength

The compressive strengths at 28, 91, and 270 days have been compared with control mixes (with a ratio of 1:1:3) and iron-based FRC composites of different mixes (with a ratio of 1:2:3). The characteristic compressive strength of the concrete has been taken as the strength of the concrete when discussing its strength [19, 30]. The characteristic compressive strength F_{ck} is defined as the strength of the concrete attained by 95% of specimens of the same mixture at 28 days of curing when evaluated using a 150-mm cube, maintaining a temperature of 20 ± 5°C and pH of 7, and is calculated statistically using Equation 12 [90]. After attaining the curing age, the cubes were taken out of the water, cleaned/dried, and placed in a compressive testing machine resting on the smooth faces as per BS EN 12390-3:2019 [91]. A uniform hydraulic load of 0.6 KN ± 0.2 per second was applied until the occurrence of the failure of the cube. The maximum load P was noted in "Newtons N" from the machine to calculate the compressive strength f_c using Equation 13. Mean compressive strength was then calculated using the mean of the strengths of identical cubes.

$$F_{ck} = 0.8 \times f_{average} \qquad (12)$$

$$\text{Compressive strength}\left(f_c\right) = P/A \qquad (13)$$

where f_c is the compressive strength in N/mm² or MPa, P is the load in N, and A is the area of the cube (100 × 100 mm²).

A target characteristic compressive strength of 40 MPa for C32/40 or M40 concrete was set for this study (represented with a red line on graphs). Generally, all the NAFRIC-based composites achieved the target strength at 28, 91, and 270 days except for a few mixes of 2% WSF with 20% PA, which exhibited less than 40 MPa strength at 28 days (**Figure 5**). The least compressive strength of 37 MPa was demonstrated by the NAFRIC containing 20% PA and 2% WSF at 28 days of curing. The maximum compressive strength of 70 MPa was exhibited by ternary Fe-based composites containing 10% PFA + 10% GGBS and 10% STF at 270 days of curing. An overall increasing trend in compressive strength was observed with the increased age of curing from 28 to 270 days, espousing the completion of slow pozzolanic reaction over an extended curing period and suggesting a practical use of Fe-based FRC composites on the waterfront/hydraulic structures. Established fibers of STF with 10–17% dosage and PPF with 1–2% dosage performed exceptionally well, as expected, by demonstrating 60–70 MPa strength at par with the high-strength concrete at 91 and 270 days of curing. The innovative PET fibers also performed at par with the established fibers, exhibiting a high strength performance of 60–66 MPa at 91/270 days of curing. However, WSF demonstrated the least compressive strength with all Fe-based composites, though still achieving C32/40 or M40 strength with 1%, suggesting its feasible use for low-strength applications. All the NAFRIC mixes with fibers performed better than the PCC control (ratio 1:1:3), at par or slightly lesser than the NAFRIC control mixes (without fibers in ratio 1:2:3), suggesting the feasible use of NAFRIC SCMs.

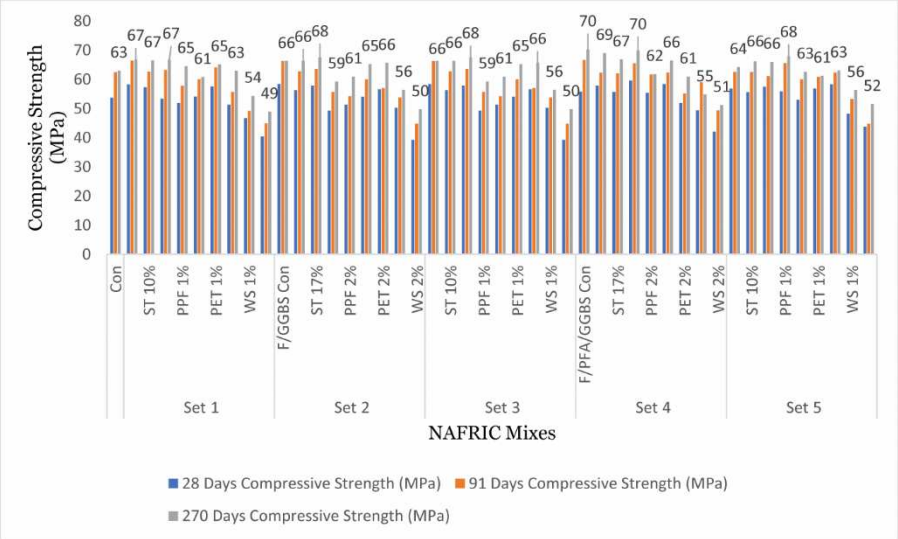

Figure 5 • Comparison of compressive strength—NAFRIC mixes at 28, 91, and 270 days of curing. All the mixes achieved 50–70 Mpa strength with a slight decrease due to the incorporation of fibers with wheat straw fibers in some mixes.

4.4. Flexural strength and post-crack ductility

The flexural strength of concrete is a significant engineering property that assesses the material's ability to withstand the bending load against rupture. It is generally considered equal to 7–10% of the compressive strength of concrete [33]. Equation 14 was then used to determine the flexural strength/transverse modulus of rupture as per BS EN 12350-1 [87] to determine the ductility of the material to withstand the rupture on bending forces caused by direct forces, spalling/thawing, warping, or angular application of loading on different elements of construction.

$$\text{Flexural strength}\left(f_{\text{f}}\right) = \left(3Pl\right)/\left(2bd^2\right) \quad (14)$$

where f_f = flexural strength in N/mm² or MPa, P = load in "N" Newtons, l = length of the prism (500 mm), b = width of the prism (100 mm), and d = depth of prism (100 mm).

The results have been compared with prisms made of the PCC control mix with a ratio of 1:1:3, the NAFRIC control mixes (without fibers, mix ratio 1:2:3), and NAFRIC composites (with fibers, mix ratio 1:2:3), as shown in **Figure 6**. A 100% increase in 10% STF-based Fe composite with 20% PFA exhibiting 8.6 MPa flexural strength has been observed compared to the control mixes (4.3 and 4.4 MPa). The maximum flexural strength of 8.3–8.9 MPa (around 123% increase versus the control mixes) has been demonstrated by set 4 mixes containing ternary pozzolans of 8% MK and 10% PFA + 10% GGBS with STF 10% and 17%. Overall, 10% and 17% STF performed the best, with all pozzolanic Fe-based mixes attaining an increase of 72–123% in flexural strength. 1% PPF and 1% PET fibers performed comparably well, achieving 6.8–7.9 MPa strength (up to 70% increase); the NAFRIC with 20% PA demonstrated 7.6–7.9 MPa strength with 1–2% PET fibers, suggesting at par use of innovative waste PET bottle fibers as disposal of waste option with an improvement of flexural strength of NAFRIC SCMs [1, 19, 92]. When a flexural/bending force is applied on a prism at a three-point loading machine, the failure crack starts appearing almost at the mid-point in the bottom layer, which keeps widening/increasing in displacement with increased loading. When an element is subject to a bending load, its upper portion experiences compression and the lower portion experiences a tensile force that tries to pull it out while bent on the loading point (**Figure 7**). A ductile material like steel or plastic will exhibit a unique behavior showing extended displacement/crack widening instead of sudden rupture before failure with a slightly decreasing bending force or even without any bending force, known as post-crack ductility or residual ductility [1, 74, 75]. A study on the impact of different fibers on the flexural strength of FRC mixes elucidated that the PCC mixes without fibers demonstrated an abrupt rupture when bending forces were applied to three-point loading in the flexural testing machine. However, the mixes with the fibers exhibited post-crack ductility even after rupture/failure by showing displacement/widening of the crack. The same analogy has been observed with NAFRIC mixes, as adding iron powder increases composites' ductility/flexural strength better than PCC, as elucidated in **Figure 8**. The control mix ruptures without post-crack ductility, exhibiting a displacement/crack width of 5 mm on rupture (**Figure 8a**). The incorporation of fibers increased the post-crack ductility of composites. The prisms remained intact even after showing a crack/displacement of around 43–54 mm, exhibiting very high post-crack ductility and increased flexural strength of FRC mixes, as shown in **Figure 8b** and **8c** (graphs showing a relationship between flexural strength/displacement and comparison of the control mix's abrupt rupture with the ductile rupture of the best performing NAFRIC SCMs containing established 10% STF and novel 1% PET).

4.5. Carbonation testing using phenolphthalein

In this study, a carbonation test has been conducted to determine the consumption of CO_2 during the hydration process to produce $FeCO_3$ in iron-based binary/ternary pozzolanic composites. If the phenolphthalein spray turns light pink or remains colorless, then it means that iron powder has consumed CO_2 absorbed during the carbonation process and has even reacted with limestone $CaCO_3$ to convert itself into rock-like $FeCO_3$, giving enhanced strength to the materials and fully converting CaO and SiO_2 into C-S-H gel. This phenomenon supports using Fe powder with pozzolans and $CaCO_3$ to produce high-strength SCMs with low-carbon, greener construction materials for better environmental impacts and to reduce the carbon footprints of the construction industry [93, 94]. The OPC-based composites demonstrated a dark pink color at 28 days, exhibiting the presence of a large quantity of CO_2, which gradually reduced to a lesser pink area at

91 days and even less at 270 days but still present significantly at deeper segments and areas showing containment of embodied CO_2 (**Figure 9a**). All the specimens of NAFRIC demonstrated colorless or a very light pink color at 28, 91, and 270 days of curing/applying phenolphthalein spray (**Figure 9b**). NAFRIC specimens absorbed the CO_2 to form $FeCO_3$ in the reaction of iron and CO_2, suggesting them to be carbon-absorbent materials. Negligible/very few traces of pink color were visible on the cubes after 270 days of curing, supporting the achievement of the increased strength, full completion of carbonation reaction, and absorption of CO_2, making them greener, eco-friendly, and sustainable materials compared to the cement-based concrete.

Figure 6 • Comparison of flexural strength—NAFRIC mixes. A 70–120% increase was observed in flexural strength compared to the PCC 1:1:3 control mix.

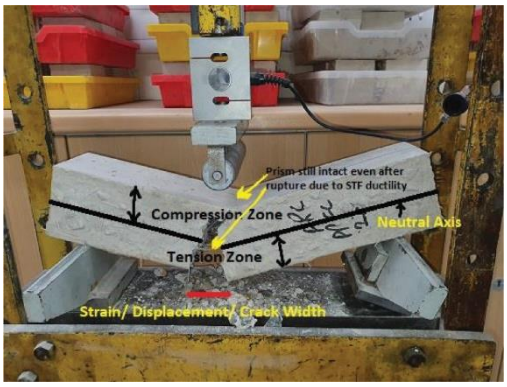

Figure 7 • Mechanism of modulus of rupture and post-crack ductility in fiber-reinforced prisms during flexural strength testing.

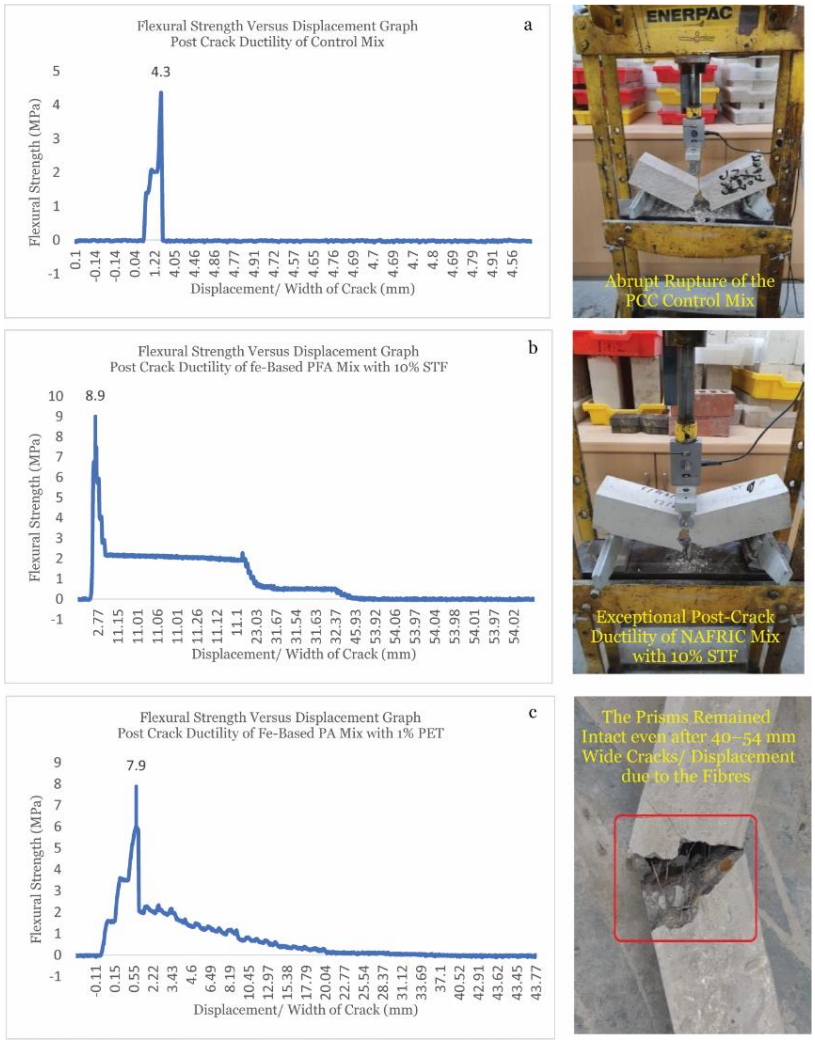

Figure 8 • Flexural strength versus displacement graph—post-crack ductility: (a) control mix, (b) NAFRIC 10% STF, and (c) NAFRIC 1% PET fibers mixes. The control mix ruptures without post-crack ductility (a). The incorporation of fibers increased the post-crack ductility of composites, showing a crack/displacement of around 43–54 mm, exhibiting very high post-crack ductility and increased flexural strength of FRC mixes, as shown in parts (b) and (c). The presence of fibers in the specimen strengthens the specimen to reinforce against surface cracks, improves structural refinement/bonding against bending forces, and increases ductility. However, it is not a substitute for steel reinforcement, but it can increase flexural strength compared to plain concrete.

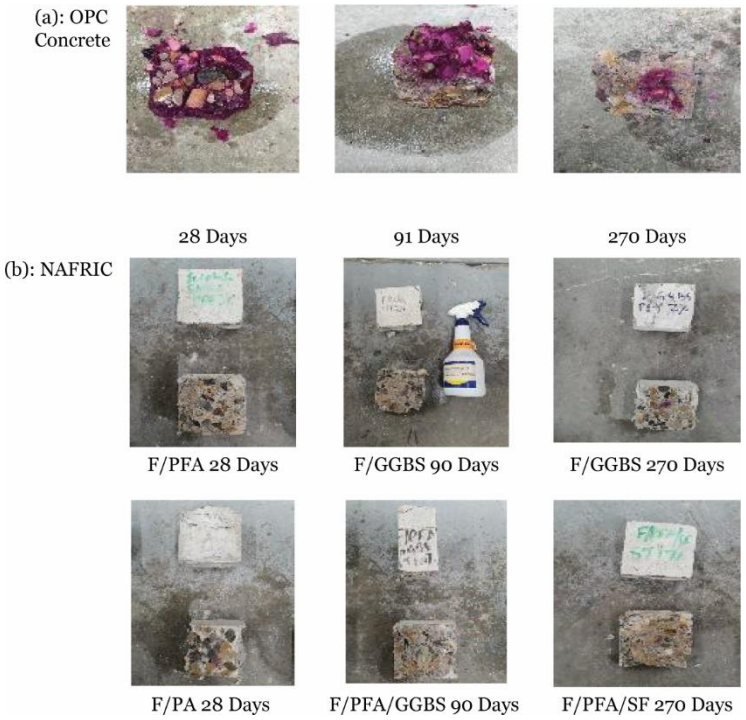

Figure 9 • Carbonation testing using phenolphthalein and assessing the presence/absorption of CO_2 (a: pink color—CO_2 present, b: for different NAFRIC SCMs: light pink or no color—no or less CO_2 present/CO_2 absorbed to convert to $FeCO_3$).

4.6. Durability of NAFRIC composites against sulfate attack

The chemo-mechanical synthesis of sulfate attack has been discussed in Section 1.5 (Equations 7–10). The NAFRIC composites containing iron powder improve pore refinement and provide surface protection to prevent the ingress of chemicals due to hard rock-like siderite $FeCO_3$. The mixing of pozzolans with OPC is considered beneficial as a filler material, which results in pore refinement, reduced voids, formation of the additional quantity of C-S-H gel during the pozzolanic reaction, consumption of portlandite to convert to C-S-H gel, and reduction of ettringite formation and M-S-H gel at the later stage. However, using fibers incorporates weaker failure plains and reduced intra-ingredient binding and can help produce/propagate the ettringite crystal cracks along the fibers. Excess use of pozzolans can result in the swelling of $Si(OH)_4$, and $MgSO_4$ can exchange cations with C-S-H gel to form ettringite and mushy M-S-H gel after the sulfate attack. The hard rock-like characteristics of $FeCO_3$ prevent the Na_2SO_4-specific sulfate attack, resulting in elongation. The iron-based pozzolanic binary composites with PFA and MK were considered to withstand the sulfate attack with minimum elongation, surface deterioration, and loss of strength. The cubes were analyzed for surface deterioration, and a qualitative classification of 0–5 scores was used for total/partial damage, pitting/cracking, surface attack, side/corner damage, and discoloration. Generally, all the NAFRIC composites remained intact and composed after the 270 days of accelerated sulfate attack and demonstrated very mild discoloration and mild pitting/cracking; no sides or corner damages were observed, no specimen exhibited total/partial damage, and the surface of all the specimens remained intact, all demonstrating a very mild impact score of 0–2 (**Table 3** and **Figure 10**). The salt deposition was observed on a few points in a few specimens, and the control mixes and a few mixes with WSF and composites with increased dosages of 2% fibers showed very mild surface deterioration.

Table 3 • Deterioration at 270 days of sulfate attack—NAFRIC SCMs

	Total damage	Partial damage	Surface attack	Pitting/cracking	Corner damage	Decoloration
	Qualitative scoring 0–5					
Con	0	0	2	2	1	2
ST 10%	0	0	2	2	1	2
ST 17%	0	0	2	2	1	2
PPF 0.5%	0	0	2	2	1	2
PPF 1%	0	0	2	2	1	2
PPF 1.5%	0	0	2	2	1	2
PPF 2%	0	0	2	2	1	2
Coir 0.5%	0	0	2	2	1	2
Coir 1%	0	0	2	2	1	2

Coir 1.5 %	0	0	2	2	1	2
Coir 2%	0	0	2	2	1	2
PET 0.5%	0	0	2	2	1	2
PET 1%	0	0	2	2	1	2
PET 1.5%	0	0	2	2	1	2
PET 2%	0	0	2	2	1	2
WS 0.5%	0	0	2	2	1	2
WS 1%	0	0	2	2	1	2
WS 1.5%	0	0	2	2	1	2
WS 2%	0	0	2	2	1	2

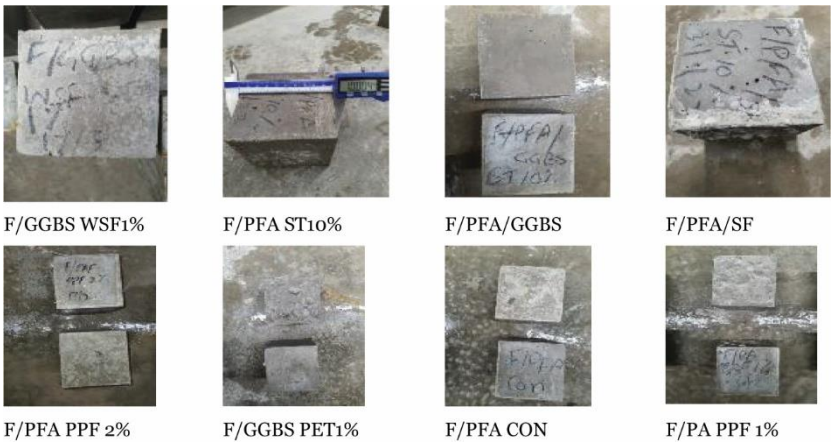

Figure 10 • Qualitative analysis and physical deterioration in NAFRIC composites after 270 days of sulfate attack (very mild discoloration and slight pitting/cracking observed).

4.6.1. The elongation/length variation index

The elongation/length variation index was calculated using the length of water-cured cubes versus the length of cubes after 270 days of sulfate exposure to determine the durability of the specimens, considering the Na_2SO_4-triggered elongation, using Equation 15 [25, 26, 45]. The elongation/length variation index was calculated using Equation 14:

$$\text{Length variation index}(\%)\,(\Delta L) = \left[\left(L_s - L_i\right)/L_o\right] \times 100 \quad (15)$$

where ΔL is the length variation index in %age and L_i is the initial length of the cube face on immersion, L_s is the length of the same cube surface after 270 days of immersion in a sulfate solution, and L_o is the inner dimension of the originalmold. A negative index shows reduction, and a positive index shows elongation in length. Elongation results from Na_2SO_4 attack due to spalling/expansion caused by exchange of cations (Ca^{++} and Na^{+}) with anions (SO_4^{--} and OH^{-}). All the NAFRIC composites exhibited mild elongation due to the Na_2SO_4 attack ranging from 0.04 to 0.09%. The maximum elongation was observed in PCC control of 0.10%, followed by F/PFA control of 0.09%. All other control mixes of NAFRIC composites exhibited 0.07–0.08% elongation. The maximum elongation of 0.09% was exhibited by a few specimens of WSF with GGBS and PFA-based NAFRIC composites. PA-based NAFRIC composites elongated 0.05–0.07% with all the fibers, suggesting they were the best iron-based binary pozzolanic NAFRIC composite material. The traditional PFA + MK-based binary pozzolanic NAFRIC exhibited the maximum elongation in a few mixes of 0.09%, suggesting it to be comparatively more impacted but still under 0.09%. The composites containing ternary pozzolans with iron (PFA/GGBS/SF with MK and lime) equally performed at par with the binary composites and showed an elongation of 0.06–0.08%, as shown in **Figure 11**.

4.6.2. Strength deterioration index (SDI)

The SDI was calculated using the strength of water-cured cubes versus the strength in the sulfate exposure of 270 days to determine the durability of the specimens considering the $MgSO_4$ triggered strength loss/ettringite formation. The compressive strength testing for all the cubes exposed in a concentrated sulfate solution tank and water tank was conducted to determine the strength variation/durability of materials by comparing them with each other and with other specimens in sulfate solution/water. The SDI was calculated using Equation 16 [25, 26, 45].

$$\text{Strength deterioration index}(\%)\,(\text{SDI}) = \left[\left(f_w - f_s\right)/f_w\right] \times 100 \quad (16)$$

where f_w is the compressive strength of water-cured cubes and f_s is the compressive strength of cubes' surface after 270 days of immersion in a sulfate solution. A negative SDI shows improved strength, and a positive index shows strength reduction.

The sulfate attack by $MgSO_4$ is characterized by the loss of compressive strength due to ettringite formation and, finally, the conversion of C-S-H gel into strengthless mushy M-S-H gel. The hard rock-like properties of $FeCO_3$ and pozzolanic reaction by the pozzolans in the SCMs consume $Ca(OH)_2$ to form additional C-S-H gel, increasing the strength. The sulfate attack specific to $MgSO_4$ reduces the compressive strength of fiber-reinforced

composites due to weaker plains/random distribution/pore disturbance. As a net result, some NAFRIC composites exhibit a gain in strength, and some show a loss in strength. Generally, all the NAFRIC composites except a few remained compact and intact in the 270 days of accelerated sulfate attack depicting 20 years of field conditions. The SDI was observed up to 2–11% in control mixes without fibers (**Figure 12**). The least performing composites belong to the traditional NAFRIC, with 20% PFA exhibiting a 3–12% SDI. The best-performing binary NAFRIC composites belong to the 20% PA-based SCMs, exhibiting an SDI of −2 to 12% (negative value means strength gain in sulfate solution), followed by 20% GGBS-based composites showing an SDI of 2–11%. The best-performing ternary pozzolanic NAFRIC composites belonged to 10% PFA + 10% SF, exhibiting an SDI of 6–11%, followed by 10% PFA + 10% GGBS composites showing −2 to 12% SDI. Overall, most NAFRIC composites demonstrated an SDI of less than 10%, which is well within the 10% strength variation and can be considered as maintaining their strength in a 20-year field depicted sulfate attack.

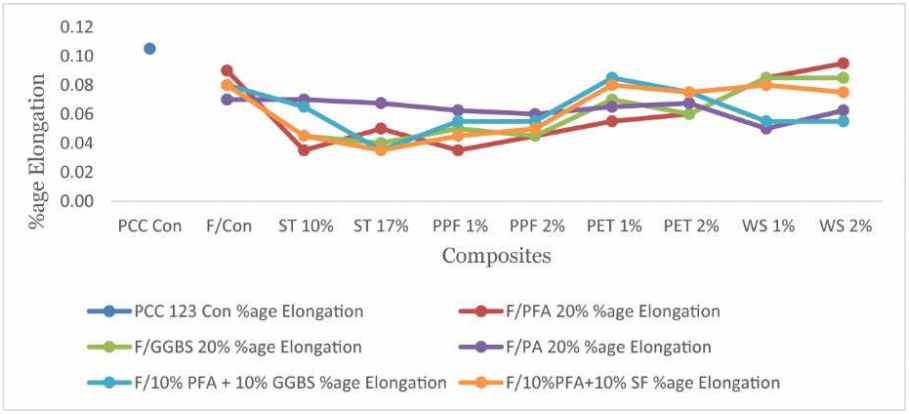

Figure 11 • Percentage elongation of NAFRIC composite cubes after 270 days of sulfate attack (a negligible 0.05–0.1% elongation was observed, PCC control mix was observed most affected, and all the NAFRIC mixes were observed as least affected by Na_2SO_4 elongation attack).

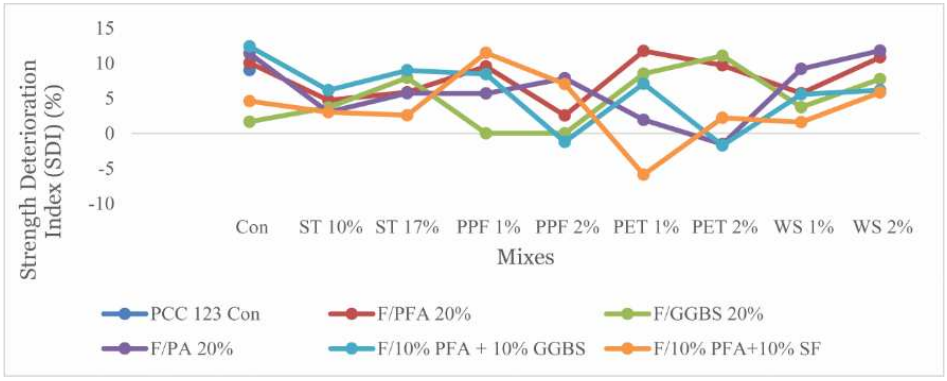

Figure 12 • Comparison of strength deterioration index (SDI (%))—NAFRIC mixes, after $MgSO_4$ sulfate attack (a negative SDI shows improved strength, and a positive index shows strength reduction). All the mixes exhibited a meager SDI of up to 10%, and a few improved the strength, demonstrating more durability/resistance of NAFRIC SCMs against sulfate attack.

4.7. Microstructural studies using XRD, XRF, SEM, and EDAX

4.7.1. Microstructural analysis using XRF/XRD

The XRF in **Table 4a** shows that the specimens contained 33–33.7% SiO_2 due to pozzolans and 50–56% CaO due to using lime and cement as the significant components identical to cement concrete and demonstrating the formation of up to 80–90% of C-S-H gel inducing a good compressive strength. Fe elements were observed as 1.45–3.7%, as expected due to GGBS and iron powder mixing in iron-based pozzolanic composites showing the formation of $FeCO_3$ and ferrites. The composites with PA contained slightly more potassium, which can cause swelling/loss of strength in the mixtures. NAFRIC composites with OPC as 90% binder contained around 4% alumina showing celite reaction (calcium aluminosilicate hydrates). The presence of a few traces of Na_2O shows a minimum impact of Na_2SO_4 during sulfate attack, whereas the presence of magnesium oxide (1.1–2.26%) and SO_3^{--} (0.4–0.9%) exhibits a very mild sulfate attack due to $MgSO_4$. **Table 4b** and **Figure 13** and **13b** (XRD spectra) show the elemental/compound composition determined by XRD/Eva software (version 6, Bruker, Billerica, MA, USA) using an XRD technique. The specimens contained rich quantities of around 40–60% quartz and 35–55% lime (on the normalized scale), predicting an excellent formation of C-S-H gel. Dolomite and pigeonite with Fe and Mg show the formation of ferrous carbonate and brucite after the sulfate attack. Less than 0.9% ettringite formation after the sulfate attack shows the durability of the material and its strength to withstand the sulfate attack with maintained/improved strength. The presence of portlandite has been observed to be minimal in NAFRIC composites. The results indicate the complete formation of C-S-H gel by utilizing a maximum quantity of CaO, SiO_2, and $Ca(OH)_2$ and leaving significantly less aqueous portlandite to initiate cationic/anionic exchange of Ca^{++}, Na^{+}, and Mg^{++} with OH^{-} and SO_4^{2-} required to initiate the sulfate attack by Na_2SO_4 and

$MgSO_4$. The XRF and XRD results support the findings about the durability/strength of the innovative NAFRIC composites by chemical-mechanical synthesis/laboratory testing and identify these as sulfate-resistant strong composites with the complete formation of strength-inducing C-S-H gel.

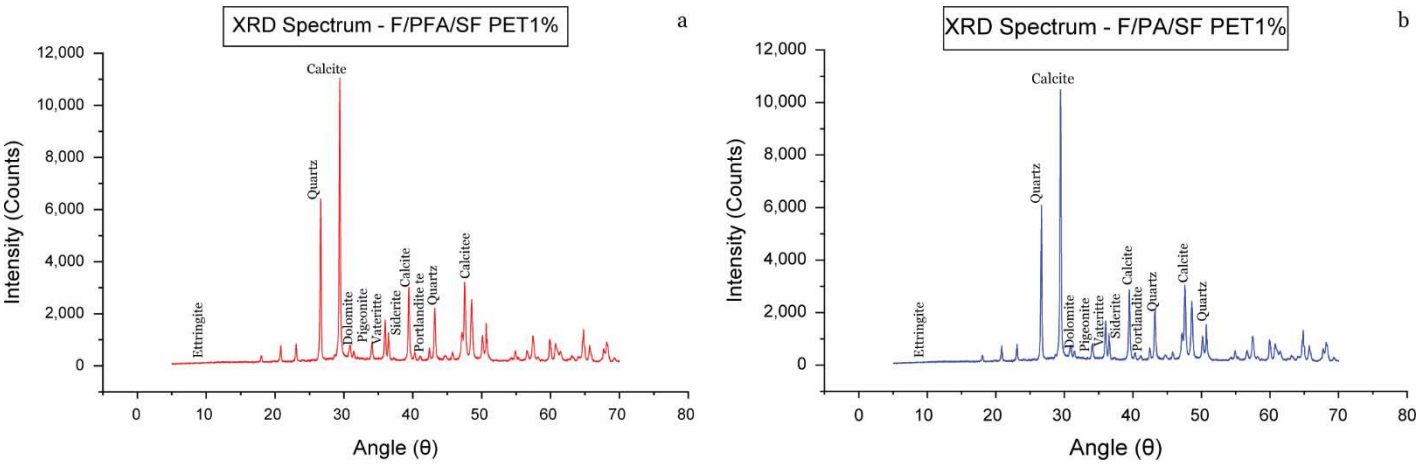

Figure 13 • XRD spectrometry—compound composition, phases/peaks of (a) F/PFA/SF PET1% and (b) F/PA PET1%. Significant, identical peaks of calcite and quartz show the excellent formation of C-S-H gel; siderite shows the formation of $FeCO_3$/absorption of CO_2; minor peaks of Dolomite and Ettringite show the minimal extent of sulfate attack by $MgSO_4$.

Table 4a • Elemental composition using XRF.

Elemental composition	F/PFA/SF PET 1.0	F/PA PET 1.0
Fe_2O_3 %	2.46	3.73
SiO_2 %	33	33.7
TiO_2 %	0.27	0.3
CaO %	56.5	54.2
K_2O %	0.37	0.48
Al_2O_3 %	3.62	3.81
MgO %	2.26	1.7
Na_2O %	0.27	0.2
P_2O_5 %	<0.1	<0.1
SO_3 %	0.52	0.95
Cl %	0.12	0.41
Cr_2O_3 %	<0.1	<0.1
MnO %	<0.1	<0.1
SrO %	0.12	0.11

Table 4b • Elemental compound composition NAFRIC SCMs using XRD/Eva software

Elemental compound composition using XRD/Eva software							
		Quartz (SiO_2)	Calcium carbonate ($CaCO_3$)	Dolomite ($CaMg_{0.77}Fe_{0.23}(CO_3)_2$)	Lime (CaO)	Portlandite ($Ca(OH)_2$)	Ettringite ($3CaO{\cdot}Al_2O_3{\cdot}3CaSO_4{\cdot}32H_2O$)
F/PFA/SF PET 1.0%	Eva	59.90%	35.10%	2.40%		2.60%	<0.01%
	Y-axis	100	56.92	4.65		4.88	<0.4
	Normalized	60.08	34.2	2.79		2.93	<0.3
F/PA PET 1.0%	Eva	37.10%	55.10%	2.70%	0.30%	4.70%	<0.01%
	Y-axis	79.5	100	7.51	0.12	10.5	<1.1
	Normalized	40.23	50.6	3.8	0.06	5.31	<0.9

4.7.2. Microstructural analysis using EDS, EDAX, and TEM with TEAM software

The microstructural analysis using EDS, EDAX, and transmission electron microscopy (TEM, ThermoFisher Scientific Scientific, Waltham, MA, USA) with TEAM software (AMETEK, Inc., Berwyn, PA, USA), which augmented the research findings that the development strength is due to extensive formation of C-S-H gel with all over-spread in the specimen. The failure/loss of strength in concrete is attributed to the formation of ettringite, gypsum, brucite, M-S-H gel, portlandite, expansive silica hydroxide gel, and carbonation of metal hydroxides due to internal/external sulfate attacks on samples having more water-cement ratio and exposed to more concentrated magnesium/sodium sulfate solutions. Microstructural study of materials is an essential/advanced method of investigating the morphology, shape, pattern, type alignment, elemental composition, and quantity assessment/mapping of various chemicals identified using X-ray and electron beams. X-rays or electrons are made to strike with the target testing material specimen to scatter the electrons from the K, L, and M electron orbits with specific intensity and scattering angles θ, releasing specific energy photons characteristically identical for each element/compound matching it to the American Mineralogist Crystal Structure Database (AMCSD) to create spectrums/images [95, 96]. **Figure 14a** shows a combined identical spectrum illustrating the coinciding peaks of different NAFRIC SCMs; **Figure 14b** and **14c** illustrates individual spectrums of two NAFRIC specimens (F/PFA/SF PET1% and F/FA PET1%). These EDS spectrums show two significant major and minor peaks of Ca and Si. The Ca peak is more extensive than Si, showing more composition of C-S-H gel and $Ca(OH)_2$. Fe peak shows the formation of $FeCO_3$. The minor Mg and S peaks show the presence of brucite and ettringite but in minimal quantities, elucidating the sustainable use of strong NAFRIC composites as durable sulfate-resistant materials. The NAFRIC composites were found to contain a residual amount of portlandite. Increasing pozzolanic material may likely increase strength as the quantity of Si from increased pozzolan and residual portlandite can presumably be converted into additional C-S-H gel. However, the findings of this research that iron-based binary and ternary pozzolanic composites are more robust and durable than cement concrete are reassured by the microstructural analysis, which aligns with the findings of the mechanical properties of NAFRIC SCMs. The microstructural analysis conducted using XRF, XRD, and EDS is further supported by studying specimens through EDAX and TEM using TEAM software on an SEM machine. TEAM provided a colored dispersal mapping of elements present on the specimen with different color coding and phase identification. **Figure 15a** and **15b** shows the elemental mapping with color coding for the electrons scattered from the K orbit phase. All the specimens have been mapped with up to 90% calcium and silica, showing a uniform spread and a large-scale formation of C-S-H gel with complete hydration. Negligible Mg and S formation shows a minor impact of sulfate attack with less than 2% of ettringite and brucite production. The presence of Fe shows the formation of $FeCO_3$, which is another strength and induces rock-like formation. These results were finally analyzed with SEM images of the crystals' real-time morphology and orientation. All the above analyses using XRF, XRD, EDAX, and TEM have supported the strength/durability characteristics of the innovative NAFRIC SCMs.

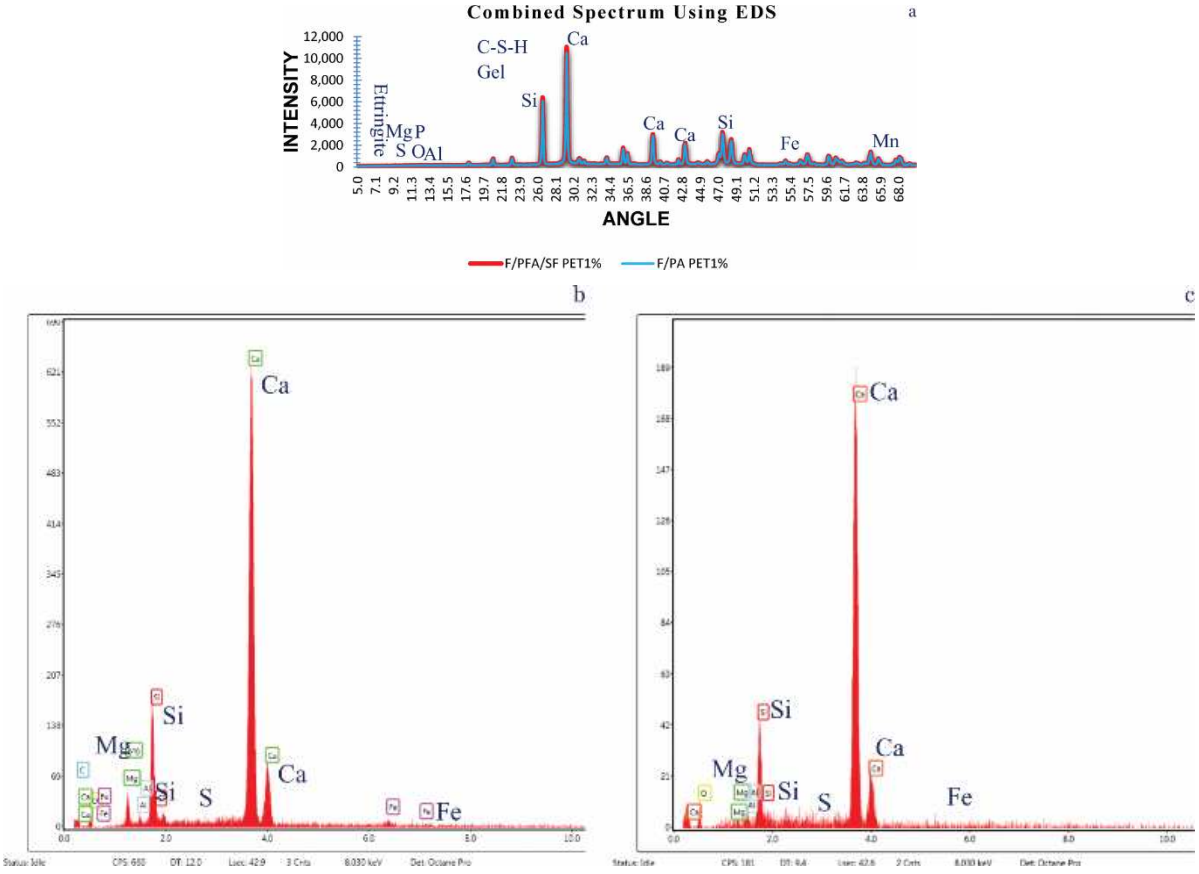

Figure 14 (a) • Combined EDS spectrum of NAFRIC mixes exhibits identical/coinciding major/minor peaks of similar behavior. (b and c) EDS spectrum of NAFRIC SCMs after sulfate attack; (b) F/PFA/SF PET1%. (c) F/FA PET1% (Ca and Si peaks have emerged as identical significant peaks exhibiting the formation of extensive C-S-H gel; minor Fe, Mg, and S peaks show the formation of $FeCO_3$, brucite and ettringite in meager quantities).

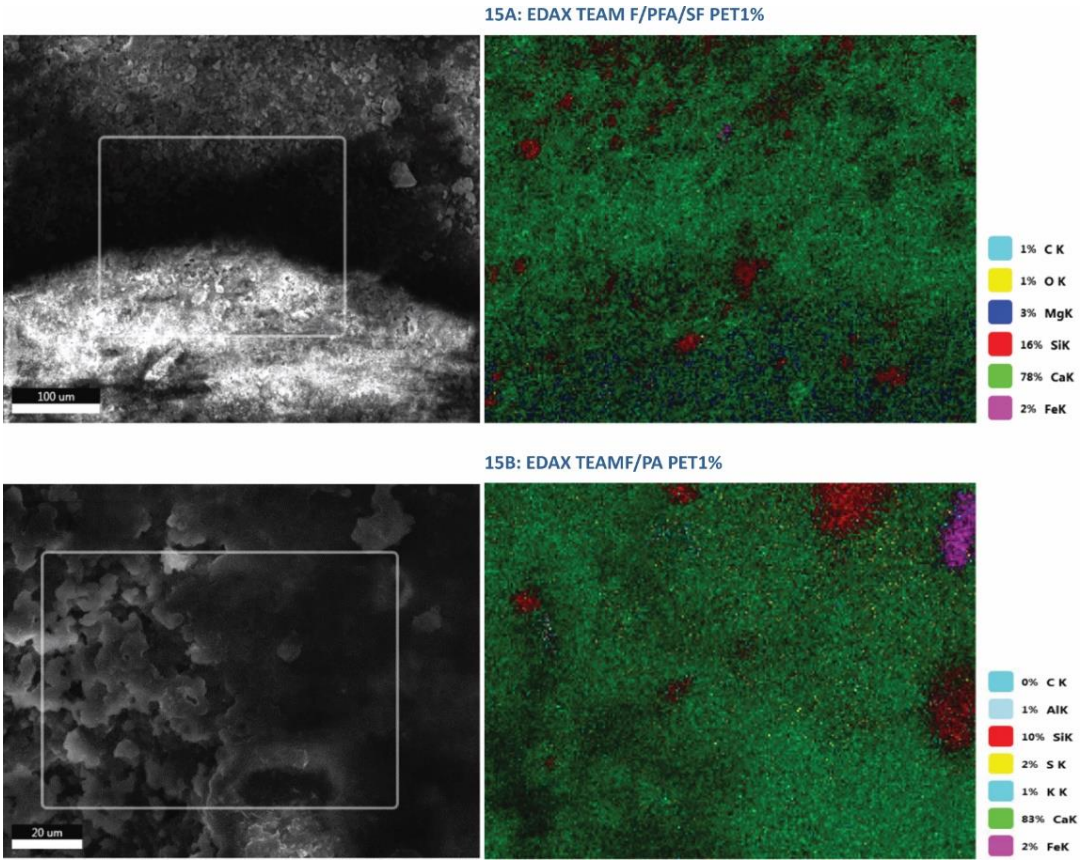

Figure 15 • Elemental mapping using EDAX-TEAM: (a) F/PFA/SF PET1% and (b) F/PA PET1%. (TEAM provided a colored dispersal mapping of elements present on the specimen with different color coding and phase identification. The specimens have been mapped with up to 90% calcium and silica, an extensive formation of C-S-H gel with complete hydration. Negligible Mg and S formation shows a minor impact of sulfate attack. The presence of Fe shows the formation of $FeCO_3$.)

4.7.3. Microstructural analysis using SEM

The SEM provides real-time imaging of the specimen generated by scatted/diffracted electron beams, with 10–25,000 magnification, 2–5 µm, using SE mode, HV of 5 kV, and angles θ–5θ on Nova Nano SEM machine. **Figure 16a** and **16b** shows the SEM images of NAFRIC composites of iron-based binary and ternary pozzolanic mixes of F/PFA/SF PET1% and F/PA PET1%. The images show that the materials have crystalline morphology. The dense formation of C-S-H gel is visible, with bigger dark gray crystals uniformly spread all over the specimen, interpreting the occurrence of a complete hydration process; the formation of additional C-S-H gel due to swift hydration of alite, belite, celite, CaO, SiO_2, and $Ca(OH)_2$; and pozzolanic reaction. Some quantity of $Ca(OH)_2$ has been observed as unutilized in the mix, which identifies a potential for additional formation of C-S-H gel and enhanced strength if pozzolans' quantity is increased. The prominent needle-like protruding crystals and the formation of C-S-H gel show the presence of $FeCO_3$ formed by a reaction of iron powder and CO_2. The untreated particles of Fe identify the room to use an additional quantity of CO_2 from the environment or may be injected into the specimen and cured in a saturated CO_2 tank for the additional formation of $FeCO_3$. The formation of calcite ($CaCO_3$) was also observed with calcium monosulfate aluminate hydrate and brucite, making an external membrane on the outer surface. A few crystals of ettringite were observed, elucidating the material's enhanced durability and capacity to withstand sulfate attack in a better way. All the advanced XRF, XRD, SEM, EDAX, TEAM, and sulfate resistance testing and microstructural analysis of NAFRIC SCMs suggest beneficial use in all types of construction applications, including their practical use in marine environments, saltish soils, hydraulic structures, and hydromodifications/flood protection defenses due to their inherent capability to withstand hazardous chemicals ingress and strength deterioration.

4.8. Assessment of embodied CO_2 and cost-benefit analysis

The NAFRIC SCMs are the high-strength concrete alternatives considered low-carbon materials due to the absorption of CO_2 by Fe to form $FeCO_3$. This study used a 10% replacement of OPC with NAFRIC SCMs, which can be increased feasibly to 50% for lower strength utilization but for better environmental impacts, provided iron powder (Fe) is available in abundance [19]. Moreover, the choice of cement alternative (GGBS) or pozzolans (PFA/SF/PA) influences the carbon absorption capability and cost of the NAFRIC material. A calculation of embodied CO_2 and cost of materials has been conducted using the characteristic embodied CO_2 and cost of each constituent material using ICE database version 3 of circular ecology [97, 98] and market values to conduct a cost-benefit analysis, as shown in **Table 5**. 10–50% iron-based pozzolanic NAFRIC composites can exhibit a reduced embodied CO_2 by 7–92% but with up to 17–86% increased construction cost and slightly reduced strength. Iron powder is is available in limited supply and involves transportation costs from the steel industry to construction industries/sites, making it costly. Its high-strength achievement and 7–83% reduced embodied CO_2 make it an ideal construction material. NAFRIC with a 1:2:3 mix ratio can achieve a high strength at par/more than 60–70 MPa, exhibited by a 1:1:3 cement concrete mix ratio. It can save on the quantity of cement, reduce construction

industry emissions, and gain high strength with even 10–50% more absorption of CO_2 with increased dosages, as shown in **Table 5**. A calculation of embodied CO_2 and cost of materials has been conducted using the characteristic embodied CO_2 and cost of each constituent material using ICE database version 3 of circular ecology [97, 98] and market values to conduct a cost-benefit analysis, as shown in **Table 5** and **Tables A1–A3** in Supplementary materials. 10–50% NAFRIC with 20% GGBS-based composites exhibited 10–85% reduced emissions with 17–86% increased construction cost. 10–50% NAFRIC with 20% PFA and PA-based composites demonstrated a 10–91% reduction in embodied CO_2 but increased the cost by 8–86%. The iron-based ternary pozzolanic NAFRIC composites with 10% PFA and 10% GGBS/10% SF reduced CO_2 emissions by 7–92% but increased the cost by 17–86%. The high-strength performance, up to 90% reduction in GWP, durability in sulfate attack, and utilization in all types of construction applications make it an ideal, greener, and sustainable material if its increased cost and low availability can be compromised on its environmental benefits and lower carbon footprints to attain lower CO_2 emissions' targets.

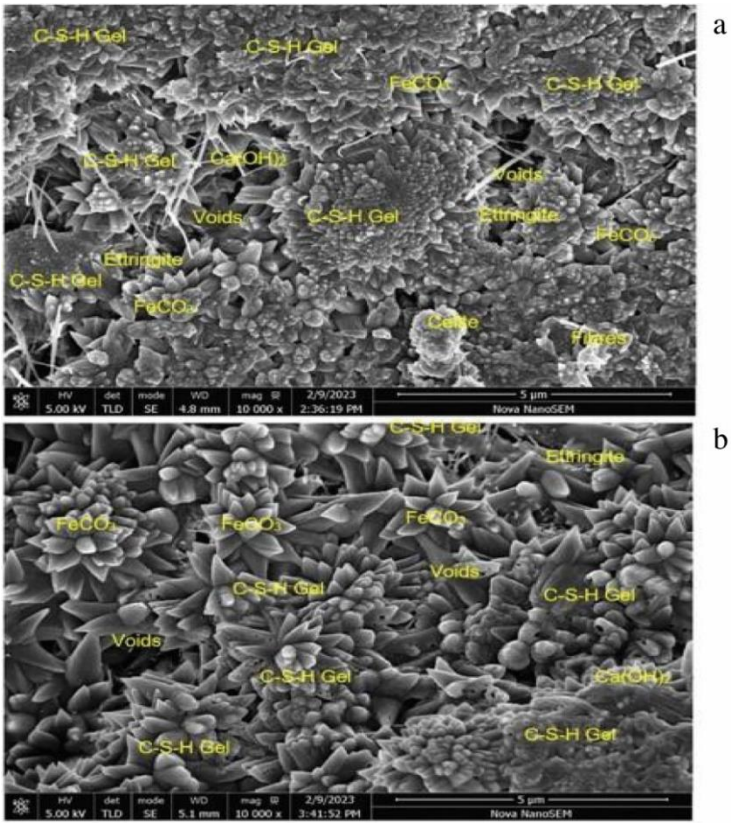

Figure 16 • (a) SEM image—F/PFA/SF PET1%, (b) SEM image—F/PA PET1%. SEM images show an excellent formation/spread of C-S-H gel all over the internal structure with hard-rock-like $FeCO_3$ formation to induce higher strength and protection against external sulfate attack.

Table 5 • Embodied CO_2 and cost-benefits of NAFRIC composites

Mix material	Total $kgCO_2e/m^3$	%age Saving of $kgCO_2e$/ton or m^3	%age Saving in cost/m^3
PCC Control	275	0	0
NAFRIC 10% with GGBS 20%	249	10	−17
NAFRIC 20% with GGBS 20%	224	23	−34
NAFRIC 30% with GGBS 20%	199	38	−52
NAFRIC 40% with GGBS 20%	174	58	−69
NAFRIC 50% with GGBS 20%	149	85	−86
NAFRIC 10% with PFA 20%	254	8	−17
NAFRIC 20% with PFA 20%	228	20	−34
NAFRIC 30% with PFA 20%	203	36	−52
NAFRIC 40% with PFA 20%	177	55	−69
NAFRIC 50% with PFA 20%	143	92	−86
NAFRIC 10% with PA 20%	251	9	−17
NAFRIC 20% with PA 20%	226	21	−34

NAFRIC 30% with PA 20%	201	37	−52
NAFRIC 40% with PA 20%	177	56	−69
NAFRIC 50% with PA 20%	152	81	−86
NAFRIC 10% with PFA 10% + GGBS 10%	257	7	−17
NAFRIC 20% with PFA 10% + GGBS 10%	232	19	−34
NAFRIC 30% with PFA 10% + GGBS 10%	207	33	−52
NAFRIC 40% with PFA 10% + GGBS 10%	170	62	−69
NAFRIC 50% with PFA 10% + GGBS 10%	145	90	−86
NAFRIC 10% with PFA 10% + SF 10%	252	9	−17
NAFRIC 20% with PFA 10% + SF 10%	226	22	−34
NAFRIC 30% with PFA 10% + SF 10%	201	37	−52
NAFRIC 40% with PFA 10% + SF 10%	175	57	−69
NAFRIC 50% with PFA 10% + SF 10%	150	83	−86

Positive values of %age savings of $kgCO_2e$/ton or m^3 show more significant environmental benefits than cement concrete. Negative cost values show more material cost than cement concrete (as per UK market rates).

5. Conclusions

Generally, all the NAFRIC in a 1:2:3 ratio mixes performed better than the cement concrete with a 1:1:3 ratio, demonstrating better durability, engineering properties, reduced embodied CO_2, and lesser use of OPC. Incorporating fibers in the Fe-based pozzolanic mixes slightly reduced the compressive strength in some mixes. Still, the overall ductility and flexural strength of NAFRIC mixes improved from 70 to 120%, elucidating the feasible use of fibers with Fe-based composites. The embodied CO_2 calculations reassured the NAFRIC SCMs as a sustainable, eco-friendly, greener waste absorbent material, with 10–12% reduced CO_2 emissions for 10% OPC replacement. The increased dosages of NAFRIC from 10% to 50% exhibited up to 17–86% reduction in the embodied CO_2. NAFRIC, with a dosage of more than 10%, can be a good cement alternative, subject to the availability of iron powder and the acceptance of increased cost versus the environmental benefits for medium-strength applications. Chemo-mechanical synthesis and microstructural analysis using SEM/XRD/TEAM/EDAX supported the evidence of NAFRIC composites' excellent resistance to sulfate attack by the 5% concentrated Na_2SO_4 + $MgSO_4$ solution. Less than 8% strength reduction was observed after 270 days of sulfate attack. A few composites improved strength by up to 7% in sulfate solution due to $FeCO_3$ and GGBS (much better performance than PCC, which reduced strength to 30% after sulfate attack). The study concludes the sustainable durability of iron-based binary/ternary pozzolanic NAFRIC composites. It suggests all the NAFRIC composites with 10–17% STF, 1–2% PPF, PETF, and WSF are sustainable, greener, and eco-friendly materials, which can be used as cement alternatives for medium-to-high-strength (40–70 MPa) construction applications in all type of structural, hydraulic, marine construction, and hydromodifications/channel stabilization/flood defenses especially in sulfate-rich environments/strata without the use of high-sulfate resistant cement contents.

Acknowledgments

The authors thank the Leeds Beckett University for making necessary arrangements to provide testing materials and advance testing opportunities using SEM/XRD.

Funding

The authors declare no financial support for the research, authorship, or publication of this article.

Author contributions

Conceptualization, H.M.N.; methodology, H.M.N.; validation, H.M.N.; formal analysis, H.M.N.; investigation, H.M.N. and I.M.; data curation, H.M.N. and I.M.; writing—original draft preparation, H.M.N.; writing—review and editing, H.M.N.; visualization, A.A.; supervision, A.A.; project administration, A.A. All authors have read and agreed to the published version of the manuscript.

Conflict of interest

The authors declare no conflict of interest.

Data availability statement

Data supporting these findings are available within the article, at https://doi.org/10.20935/AcadMatSci7277, or upon request.

Institutional review board statement

Not applicable.

Informed consent statement

Not applicable.

Sample availability

The authors declare no physical samples were used in the study.

Supplementary materials

The supplementary materials are available at https://doi.org/10.20935/AcadMatSci7277.

Additional information

Received: 2024-04-17

Accepted: 2024-06-20

Published: 2024-07-17

Academia Materials Science papers should be cited as *Academia Materials Science 2024*, ISSN 2997-2027, https://doi.org/10.20935/AcadMatSci7277. The journal's official abbreviation is *Acad. Mat. Sci.*

Publisher's note

Copyright

References

1. Nadir HM, Ahmed A. Comparative evaluation of potential impacts of agricultural and industrial waste pozzolanic binders on strengths of concrete. J Mater Sci Manuf Res. 2021;2:1–8. doi:10.47363/jmsmr/2021(2)119
2. Joshua C, Nadir HM, Ahmed A, Yates C, Yates L, Limbu N, et al. Potential sustainable cement free limecrete based on ggbs & hydrated lime as an alternative for standardised prescribed concrete applications. Res Dev Mater Sci. 2021;15(5):1753–63. doi:10.31031/rdms.2021.15.000874
3. Gagg CR. Cement and concrete as an engineering material, historical appraisal and case study analysis. Eng Fail Anal. 2014;40:114–40.
4. Ahmed A, Kamau J, Pone J, Hyndman F, Fitriani H. Chemical reactions in pozzolanic concrete. Mod Approaches Mater Sci. 2019;1(4):128–33.
5. Mineral Products Association. Embodied CO_2 of UK Cement, additions and cementitious material. Fact Sheet 18. 2007 [Part 1]:8. [cited 2024 Jan 31]. Available from: https://cement.mineralproducts.org/MPACement/media/Cement/Publications/Fact-Sheets/FS_18_Embodied_CO2e.pdf
6. Siddique R, Klaus J. Influence of metakaolin on the properties of mortar and concrete: a review. Appl Clay Sci. 2009; 43(3–4):392–400.
7. Brander M, Davis G. Greenhouse gases, CO_2, CO_2e, and Carbon: what do all these terms mean? Econometrica, White Papers. 2012 [cited 2024 Jan 26]. Available from: https://scirp.org/reference/referencespapers.aspx?referenceid=3174668
8. Widera B, Stone D. Analysis of the possible application of iron-based substitute for Portland cement in buildings and its influence on carbon emissions. The examples of Jizera Mountain region and the Tohono O'odham Indian Reservation. International Multidisciplinary Scientific GeoConference: SGEM, Sofia, Bulgaria; 2016. p. 455–62.
9. Hoornweg D, Bhada-Tata P. What a waste a global review of solid waste management - knowledge papers. 2012 [cited 2023 Jan 30]. Available from: https://documents1.worldbank.org/curated/en/302341468126264791/pdf/68135-REVISED-What-a-Waste-2012-Final-updated.pdf
10. Jo S, Pilakoutas L (Skanska), Kanavaris F, Janota M, Gibbons O, Chang L, et al. Buildings & Infrastructure Priority Actions for Sustainability. Embodied carbon concrete. ARUP. Reference: 07762000-RP-SUS-0003; 2023 [cited 2024 Jan 4]. Available from: https://www.istructe.org/IStructE/media/Public/Resources/ARUP-Embodied-carbon-concrete_1.pdf
11. Garside M. Global cement industry – statistics and facts. Statista. 2022 Oct 22 [cited 2024 Jan 26]. Available from: https://www.statista.com/topics/8700/cement-industry-worldwide/#topicOverview
12. Garside M. Cement production worldwide from 1995 to 2022. Statista. 2023 Apr 6 [cited 2023 Apr 23]. Available from: https://www.statista.com/statistics/1087115/global-cement-production-volume/
13. Global Cement and Concrete Association (GCCA). Availability: abundant, local and cost-effective. 2019 [cited 2024 Jan 31]. Available from: https://gccassociation.org/sustainability-benefits-of-concrete/availability/
14. GCCA. Global cement and concrete industry announces roadmap to achieve groundbreaking 'net zero' CO2 emissions by 2050. 2021 [cited 2024 Jan 31]. Available from: https://gccassociation.org/news/global-cement-and-concrete-industry-announces-roadmap-to-achieve-groundbreaking-net-zero-co2-emissions-by-2050/
15. GCCA. Global Cement and Concrete Association publishes cement industry net progress report 2023. 2023 [cited 2023 Dec 4]. Available from: https://www.globalcement.com/news/item/16655-global-cement-and-concrete-association-publishes-cement-industry-net-progress-report-2023
16. GCCA. Circular economy. 2023 [cited 2024 Jan 31]. Available from: https://gccassociation.org/sustainability-benefits-of-concrete/circular-economy/
17. GCCA. 2050 Net zero roadmap - one year on. 2021 [cited 2024 Jan 31]. Available from: https://gccassociation.org/2050-net-zero-roadmap-one-year-on/
18. Way R. Heavy dependence on carbon capture and storage is 'highly economically damaging', says the Oxford report. Smith School of Enterprise and the Environment. 2023 [cited 2023 Dec 5]. Available from: https://www.smithschool.ox.ac.uk/news/heavy-dependence-carbon-capture-and-storage-highly-economically-damaging-says-oxford-report

19. Nadir HM, Ahmed A, West J. Experimental investigation of engineering properties of iron-based binary and ternary pozzolanic supplementary cementitious materials. J Mater Polym Sci. 2023;3(1):1–13. doi: 10.47485/2832-9384.1024

20. Das S, Hendrix A, Stone D, Neithalath N. Flexural fracture response of a novel iron carbonate matrix – glass fibre composite and its comparison to Portland cement-based composites. Constr Build Mater. 2015;93:360–70.

21. Vijayan DS, Dineshkumar, Arvindan S, Shreelakshmi JT. Evaluation of ferrock: a greener substitute to cement. Mater Today Proc. 2020;22:781–7. doi:10.1016/j.matpr.2019.10.147

22. Karthika S, Leema AR, Priyadarshini G. Sustainable development on ferrock mortar cubes. J Phys Conf Ser. 2021; 2040: 012020. doi: 10.1088/1742-6596/2040/1/012020

23. Prashanth M, Gokul V, Shanmugasundaram M. Investigation on ferrock-based mortar an environment-friendly concrete. SSRN Electr J. 2019. doi: 10.2139/ssrn.3461209

24. National Center for Biotechnology Information. PubChem compound summary for CID 971, Oxalic Acid. 2023 [cited 2024 Jan 7]. Available from: https://pubchem.ncbi.nlm.nih.gov/compound/Oxalic-Acid

25. Nadir HM, Ahmed A. The mechanisms of sulphate attack in concrete – a review. Mod App Matrl Sci. 2022;5(2):658. MAMS.MS.ID.000206. doi: 10.32474/MAMS.2022.05.000206

26. Nadir HM, Ahmed A. Elucidating chemo-mechanical synthesis and microstructural study on the performance of partial cement-based concrete composites against sulphate attack – a review. Res Dev Material Sci. 2022;18(2):2065–78. doi: 10.31031/RDMS.2022.18.000935

27. Shivani AB, Nihana N, Gowri AS, Jalal H, Arjun R, Jinudarsh MSP. Experimental investigation of fe by complete and partial replacement of cement in concrete. Inte Res J Eng Technol. 2022;9:855.

28. Herath C, Gunasekara C, Law DW, Setunge S. Performance of high volume fly ash concrete incorporating additives: a systematic literature review. Constr Build Mater. 2020;258: 1–13. doi: 10.1016/j.conbuildmat.2020.120606

29. Kavitha OR, Shanthi VM, Arulraj GP, Sivakumar VR. Microstructural studies on eco-friendly and durable Self-compacting concrete blended with metakaolin. Appl Clay Sci. 2016;124–125:143–9. doi: 10.1016/j.clay.2016.02.011

30. Stutzman PE, Bullard JW, Feng P. Phase analysis of portland cement by combined quantitative X-ray powder diffraction and scanning electron microscopy. J Res Natl Inst Stand Technol. 2016;121:47. doi: 10.6028/jres.121.004

31. ASTM. American Society for Testing and Materials C1012/C1012M–15. Standard test method for length change of hydraulic-cement mortars exposed to a sulfate solution1. West Conshohocken (PA): American Society for Testing and Materials; 2015 [cited 2023 May 30]. Available from: https://www.astm.org/c1012_c1012m-18b.html.

32. Teng S, Afroughsabet V, Ostertag CP. Flexural behaviour and durability properties of high-performance hybrid-fibre-reinforced concrete. Constr Build Mater. 2018;182:504–15.

33. Yi Y, Zhu D, Guo S, Zhang Z, Shi C. A review on the deterioration and approaches to enhance the durability of concrete in the marine environment. Cem Concr Compos. 2020;113:1–14. doi: 10.1016/j.cemconcomp.2020.103695

34. ASTM. ASTM C1012/C1012M-15: 2018 (updated) standard test method for length change of hydraulic-cement mortars exposed to a sulphate Solution. 2018 [cited 2023 Oct 29]. Available from: https://www.astm.org/c1012_c1012m-15.html

35. BS EN 206:2013+A2:2021 Concrete. Specification, performance, production and conformity. 2013 [cited 2022 May 30]. doi: 10.3403/30257890. Available from: https://landingpage.bsigroup.com/LandingPage/Standard?UPI=0000000000030407978

36. Zhang T, Vandeperre LJ, Cheeseman CR. Formation of magnesium silicate hydrate (M-S-H) cement pastes using sodium hexametaphosphate. Cem Concr Res. 2014;65:8–14. doi: 10.1016/j.cemconres.2014.07.001

37. Show D. Cement || Definition, introduction, types, composition and tests. Mechanical Notes. 2020 [cited 2023 Jan 19]. Available from: https://mechanicalnotes.com/cement-definition-introduction-types-composition-and-tests/

38. Eldidamony H, El-Sokkari TM, Khalil K, Heikal M, Ahmed I. Hydration mechanisms of calcium sulphoaluminate C(4)A(3)(S)over-bar, C(4)A(S) over-bar phase and active belite beta-C2S. Ceram Silik. 2012;56:389–95.

39. Lea FM, Mason TO. Cement - the major cements: composition and properties. Encyclopedia Britannica. 2024 [cited 2024 Jan 31]. Available from: https://www.britannica.com/technology/cement-building-material

40. BS EN 197-1:2011. Cement. Composition, specifications and conformity criteria for common cements. 2011 Sep 30 [cited 2023 Jan 30]. ISBN: 9780580919640, Material Number: 30331489. Available from: https://www.en-standard.eu/bs-en-197-1-2011-cement-composition-specifications-and-conformity-criteria-for-common-cements/

41. BS EN 12620:2013. Aggregates for concrete. 2013 May 31 [cited 2023 Jan 30]. ISBN: 9780580697142, Material Number: 3021256. Available from: https://www.standardsuk.com/products/BS-EN-12620-2013

42. García A, Achaiah AT, Bello J, Donovan T. A life cycle comparison to ordinary portland cement. 2017 [cited 2023 Jan 17]. Available from: https://www.academia.edu/100394824/A_Life_Cycle_Comparison_to_Ordinary_Portland_Cement

43. Karuppasamy S, Dinesh Kumar K, Janardhan K. Experimental study on Ferrock: a life-cycle compression to ordinary portland cement. Int J Creat Res Thoughts. 2018; 6(1):2001–7.

44. MB Fibreglass. Iron powder. The manufacturing facts of Iron powder by MB Glass manufacturer. 2023 [cited 2023 Jan 30]. Available from: https://www.mbfg.co.uk/iron powder.html

45. STM C125-(2019). ASTM Committee C09.91, ASTM C125-19 Standard terminology relating to concrete and concrete aggregates. Annu B ASTM Stand. 2019;4. doi: 10.1520/C0125-15A

46. Oner A, Akyuz S. An experimental study on optimum usage of GGBS for the compressive strength of concrete. Cem Concr Compos. 2007;29(6):505–14. doi: 10.1016/j.cemconcomp.2007.01.001

47. Prasanna PK, Srinivasu K, Murthy AR. Compressive strength assessment using GGBS and randomly distributed fibers in concrete. Int J Innov Technol Explor Eng. 2019;9(2):1078–86.

48. Samad S, Shah A, Limbachiya MC. Strength development characteristics of concrete produced with blended cement using ground granulated blast furnace slag (GGBS) under various curing conditions. Sādhanā. 2017;42:1203–13.

49. Thomas M. Optimizing the use of fly ash in concrete. 2007 [cited 2022 July 12]. Available from: https://www.cement.org/docs/default-source/fc_concrete_technology/is548-optimizing-the-use-of-fly-ash-concrete.pdf

50. Wesche K. Fly ash in concrete: properties and performance. London: CRC Press; 2014.

51. Snellings R, Mertens G, Elsen J. Supplementary cementitious materials. Rev Mineral Geochem. 2012;74(1):211–78. doi:10.2138/rmg.2012.74.6

52. Wang M, Chen D, Wang H, Gao W. A review on fly ash high-value synthesis utilization and its prospect. Green Energy Resour. 2024;2:100062. doi: 10.1016/j.gerr.2024.100062

53. Aiswarya S, Prince AG, Dilip C. A review on the use of metakaolin in concrete. IRACST – Eng Sci Technol Int J. 2013;3:592–7.

54. Chrest AP. Guide to using silica fume in precast/prestressed concrete products. 1994 [cited 2022 July 12]. Available from: https://www.pci.org/PCI_Docs/Design_Resources/Guides_and_manuals/references/bridge_design_manual/JL-94-September-October_Guide_to_Using_Silica_Fume_in_Precast_Prestressed_Concrete_Products.pdf

55. Ferroglobe. Silicon metal. 2020 [cited 2024 Jan 26]. Available from: https://www.ferroglobe.com/products/silicon-metal/

56. Neville AM. Properties of concrete. 5th ed. Longman Essex: Pearson; 2011.

57. Hewlett PC. Lea's chemistry of cement and concrete. 5th ed. Oxford: Elsevier Science & Technology Books; 2004.

58. Jonida P, Ahmed A, Kamau J, Hyndman F. Palm oil fuel ash as a cement replacement in concrete. Mod App Mat Sci. 2018;1(1). doi: 10.32474/MAMS.2018.01.000102

59. Oates T. Lime and limestone. Kirk-Othmer encyclopedia of chemical technology. New York: Wiley; 2010. doi:10.1002/0471238961.1209130507212019.a01.pub3

60. Bheel N, Sohu S, Awoyera P, Kumar A, Abbasi SA, Olalusi OB. Effect of wheat straw ash on fresh and hardened concrete reinforced with jute fiber. Adv Civil Eng. 2021;2021:1–11. doi: 10.1155/2021/6659125

61. Guerrero LA, Maas G, Hogland W. Solid waste management challenges for cities in developing countries. Waste Manag. 2013;33(1):220–32. doi: 10.1016/j.wasman.2012.09.008

62. Brandt AM. Fibre-reinforced cement-based (FRC) composites after over 40 years of building and civil engineering development. Compos Struct. 2008;86(1-3):3–9.

63. Al-Salem SM, Lettieri P, Baeyens J. Recycling and recovery routes of plastic solid waste (PSW): a review. Waste Manag. 2009;29(10):2625–43.

64. Akca KR, Çakir O, Ipek M. Properties of polypropylene fibre reinforced concrete using recycled aggregates. Construct Build Mater. 2015;98:620–30.

65. Yildirim G, Saharan M, Ahmed HU. Influence of hydrated lime addition on the self-healing capability of high-volume fly ash incorporated cementitious composites. J Mater Civ Eng. 2015;27(6):04014187.

66. Qadir HH, Faraj RH, Sherwani AFH, Mohammed BH, Younis KH. Mechanical properties and fracture parameters of ultra-high performance steel fibre reinforced concrete composites made with extremely low water per binder ratios. SN Appl Sci. 2020;2(9):1–12.

67. Mohammed BH, Sherwani AFH, Faraj RH, Qadir HH, Younis KH. Mechanical properties and ductility behaviour of ultra-high performance fibre reinforced concrete: effect of low water-to-binder ratios and mi- cro-glass fibres. Ain Shams Eng J. 2021;12:1557–67.

68. Mohammadi Y, Carkon-Azad R, Singh SP, Kaushik SK. Impact re-resistance of steel fibrous concrete containing fibres of mixed aspect ratio. Construct Build Mater. 2009;23(1):183–9.

69. Saikia N, De Brito J. Use of plastic waste as aggregate in cement mortar and concrete preparation: a review. Construct Build Mater. 2012;34:385–401.

70. Ismail ZZ, Al-Hashmi EA. Use of waste plastic in concrete mixture as aggregate replacement. Waste Manag. 2008;28(11):2041–7.

71. Ahmed HU, Faraj RH, Hilal N, Mohammed AA, Sherwani AFH. Use of recycled fibres in concrete composites: a systematic, comprehensive review. Compos B Eng. 2021;215:108769.

72. Barros JAO. Steel fibre reinforced concrete: material properties and structural applications. In: Fangueiro R, editor. In Woodhead publishing series in textiles, fibrous and composite materials for civil engineering applications. Oxford: Woodhead Publishing; 2011. p. 95–155.

73. Tariq N, Al-Shafi HT, Ridha M, Abduljalel S. An experimental in-investigation on the pullout strength of straight steel bars in high-performing concrete. 2017. doi: 10.13140/RG.2.2.25316.42887. [cited 2024 July 04]. Available from: https://www.researchgate.net/publication/332593732_AN_EXPERIMENTAL_INVESTIGATION_ON_THE_PULLOUT_STRENGTH_OF_STRAIGHT_STEEL_BARS_IN_HIGH_PERFORMANCE_CONCRETE

74. Figiela B, Simonova H, Korniejenko K. State of the art, challenges, and emerging trends: geopolymer composite reinforced by dispersed steel fibres. Rev Adv Mater Sci. 2022;61(1):1–15. doi: 10.1515/rams-2021-0067/HTML

75. Adfil construction fibres. Properties of polypropylene by synthetic fibres. [cited 2022 July 12]. Available from: https://adfil.com/gb-en/

76. Singh SK. Polypropylene fibre reinforced concrete: an overview. Structural Engineering Division, Central Building Research Institute. 2016 [cited 2022 July 12]. Available from: https://www.nbmcw.com/product-technology/construction-chemicals-waterproofing/concrete-admixtures/pfrc.html

77. Reddy BBK, Tejaswini K. Strength properties of polypropylene fibre reinforced concrete. Int J Eng Res Adv Technol. 2018;4:5–12. doi:10.7324/ijerat.2018.3199

78. Laville S. Single-use plastics a serious climate change hazard, study warns. The Guardian. 2019 May 15 [cited 2024 Jul 2]. Available from: https://www.theguardian.com/environment/2019/may/15/single-use-plastics-a-serious-climate-change-hazard-study-warns?ref=marketbulletin-dotcom

79. Olam M. PET: production, properties and applications. In: Wythers MC, editor. Advances in materials science. vol. 48. New York: Nova Science Publishers, Inc.; 2021.

80. Nkomo NZ, Masu LM, Nziu PK. Effects of polyethylene terephthalate fibre reinforcement on mechanical properties of concrete. Adv Mater Sci Eng. 2022;2022:4899298.

81. Galvao JCA, Portella KF, Joukoski A, Mendes R, Ferreira ES. Use of waste polymers in concrete for repair of dam hydraulic surfaces. Constr Build Mater. 2011;25:1049–55. doi: 10.1016/j.conbuildmat.2010.06.073

82. Tufail T, Saeed F, Afzaal M. Wheat straw: a natural remedy against different maladies. Food Sci Nutr. 2021;9(4):2335–44.

83. Ruiz HA, Ruzene DS, Silva DP, Teixeira JA. Evaluation of a hydrothermal process for pretreatment of wheat straw-effect of particle size and process conditions. J Chem Technol Biotechnol. 2011;86(1):88–94.

84. O'Dogherty MJ, Huber JA, Dyson J, Marshall CJ. A study of wheat straw's physical and mechanical properties. J Agric Eng Res. 1995;62(2):133–42.

85. BSI - BS EN 8500:206-2019. Improved testing procedures for concrete. 2019 [cited 2024 Jan 27]. Available from: https://www.bsigroup.com/en-GB/industries-and-sectors/construction-and-building/bs-8500-concrete-complementary-british-standard-to-bs-en-206/

86. BSI - BS EN 12390-2. Testing hardened concrete Part 2: making and curing specimens for compressive strength tests. 2019 [cited 2024 Jan 27]. Available from: https://standards.globalspec.com/std/13376847/BS%20EN%2012390-2

87. BS EN 12350-1:2019. Testing fresh concrete. Sampling and common apparatus for flexural strength. 2019 [cited 2023 Jan 27]. Available from: https://www.en-standard.eu/bs-en-12350-1-2019-testing-fresh-concrete-sampling-and-common-apparatus/

88. CivilSir. Types of concrete grade and their ratio as per British Standard (BS). [cited 2023 Feb 6]. Available from: https://civilsir.com/types-of-concrete-grade-and-their-ratio-as-per-british-standard-bs/

89. Krishnan M. M50 concrete mix design -Steps|IS-10262: 2009 |IS-456:2000. 2021 [cited 2023 Feb 6]. Available from: https://www.eigenplus.com/detailed-calculation-of-m50-concrete-mix-design-is-102622009-is-4562000/

90. BSI. BS EN 12390-7:2019. Testing hardened concrete density of hardened concrete. 2019 [cited 2023 July 9]. Available from: https://www.en-standard.eu/bs-en-12390-7-2019-testing-hardened-concrete-density-of-hardened-concrete/

91. BSI. BS EN 12390-3:2019. Testing hardened concrete. Compressive strength of test specimens. 2019 [cited 2023 July 9]. Available from: https://www.en-standard.eu/bs-en-12390-3-2019-testing-hardened-concrete-compressive-strength-of-test-specimens/

92. Yap SP, Alengaram UJ, Jumaat MZ. Enhancement of mechanical properties in polypropylene and nylon–fibre-reinforced oil palm shell concrete. Mater Des. 2013;49:1034–41.

93. ISO1920-12:2015. 14:00-17:00. ISO. 2015 [cited 2023 Dec 9]. Available from: https://www.iso.org/standard/57932.html#:~:text=This%20procedure%20specified%20in%20ISO%201920-12%3A2015%20is%20a

94. AEIS. Carbonation test. 2023 [cited 2023 Dec 30]. Available from: https://www.aeis.com/what-we-do/specialty-field-testing/carbonation-test

95. AMCSD. rruff.geo.arizona.edu. American mineralogist crystal structure database. 2023 [cited 2023 Dec 30]. Available from: http://rruff.geo.arizona.edu/AMS/amcsd.php

96. Henry D, Eby N, Goodge J, Mogk D. Braggs Law. Geochemical Instrumentation and Analysis. 2016 [cited 2023 Dec 30]. Available from: https://serc.carleton.edu/research_education/geochemsheets/BraggsLaw.html

97. ICE V3 Database Circular Ecology. Embodied carbon training course. 2019 [cited 2023 Dec 4]. Available from: https://circularecology.com/embodied-carbon-training.html

98. ICE. Energy briefing sheet: embodied energy and carbon. Institution of Civil Engineers. [cited 2024 Jan 31]. Available from: https://www.ice.org.uk/media/w4kjrruf/embodied_energy_and_carbon.pdf